link.springer.com link.springer.com

Published online 3 February 2023 | https://doi.org/10.1007/s40843-022-2313-1
Sci China Mater 2023, 66(4): 1257–1282

Semiconductor nanomaterial-based polarized light emission: From materials to light emitting diodes

Jinlei Wu[1,2], Guoqiang Fang[2], Yongliang Zhang[1], Nandita Biswas[1], Yanan Ji[2], Wen Xu[2], Bin Dong[2*] and Ning Liu[1*]

ABSTRACT **The overall optical efficiency of backlight-based liquid crystal displays (LCDs) is less than 5% due to the loss of backlight source by polarizers, color filter, liquid crystal layer and so on. Self-emissive light emitting diodes (LEDs) have been undergoing huge development due to their substantial market potentials to meet the demand of future display. More importantly, the polarized LEDs could enhance the energy utilization efficiency by avoiding light loss caused by polarizers. Therefore, it is desirable to look for effective methods to assemble high-quality anisotropic nanomaterial films so as to fabricate polarized LEDs with high degree of polarization and external quantum efficiency. Here, the photoelectrical properties of some semiconductor nanomaterials and their potential applications for polarized LEDs are introduced. The research progress in the field of polarized light emission from materials to films and then to LEDs is reviewed. Mechanisms of polarized emission, and different assembly strategies for polarized light emitting films and LEDs are also summarized and compared. Finally, several current challenges are discussed, and perspectives on future potential commercial application of polarized LEDs are offered. We hope this review will provide a valuable summary on current status and stimulate some new insightful ideas for future development of polarized LEDs.**

Keywords: polarized LEDs, degree of polarization, external quantum efficiency, display, anisotropic nanomaterials

INTRODUCTION

It has been estimated that the display market may grow to over USD $200 billion by 2031 [1–4]. The display screens used for TV, laptop, mobile phone, tablet and smart watch take advantage of numerous technologies such as liquid crystal display (LCD), light emitting diode (LED), and organic LED. Since 1980s, LCDs have been utilized as the main display device [5,6]. Traditional LCDs rely on backlight unit display technology, which requires complex multi-layer structures, and among them vertical and horizontal polarizers are especially essential in LCD module (Scheme 1a) [6–9]. Unfortunately, the overall optical efficiency of the LCD system from the backlight source is less than 5% [7,8,10]. The polarizers and color filter are the two main LCD components responsible for the low utilization of backlight source [7,11–13]. In order to achieve more smart and precise brightness adjustment, the backlight unit of LCDs has been developed from white lamp to white LED, and then to more and smaller mini-LED backlight partitions [14–16]. Nonetheless, the color gamut and color resolution of LCDs are still far from satisfactory [17,18]. Developing new displays with high color purity, high efficiency, high resolution and wide color gamut range is an urgent issue to be addressed in the future display field.

Semiconductor nanomaterials, such as II–VI colloidal and perovskite nanomaterials are emerging as excellent luminescent materials in color display devices, due to their unique optical properties such as easily tunable emission color, narrow and symmetric photoluminescence (PL) peaks, high color purity, high PL quantum yield (PLQY), as well as their competitive low-cost solution synthesis methods [1,5,7,8,18–22]. Currently, the quantum dot enhancement film (QDEF) consisting of green and red emitting semiconductor nanomaterials dispersed in a polymer film has been widely used in backlight unit for LCD [5,7,8,18,23–25]. The QDEF plays a very important role as a photoconversion layer that can absorb blue backlight and convert the blue light into green and red light with high color purity, improving the color gamut of LCD. Sony, Samsung, TCL and LG released several flagship devices equipped with QDs to their display markets [1]. However, the QDEF still caused a quite high emitting-light power loss (>10%) due to the light absorption loss from the polymer of QDEF [5].

In addition, the process of generating polarized light in the LCD system will cause energy loss of backlight, because only the electric field parallel to the polarizer filter can pass through [7,9,11]. Therefore, the use of polarized light source can reduce light power loss when passing through the vertical polarizer filter [1]. Compared with QDs, the anisotropic nanomaterials, such as one-dimensional (1D) nanorods (NRs), 1D nanowires (NWs) and 2D nanosheets (NSs), have the advantages of low non-radiative recombination rate, high electrical conductivity, good stability, and especially good polarized light emission [13,26–31]. The anisotropic nanomaterials being randomly arranged in macro-scale have no polarized light emission properties, but the film of orientation-aligned anisotropic nanomaterials can exhibit polarization characteristics [32]. Instead of QDEF, if we integrate aligned anisotropic nanomaterials EF (ANEF) in the LCD backlight unit, the polarized light

[1] Department of Physics and Bernal Institute, University of Limerick, Limerick, Ireland
[2] Key Laboratory of New Energy and Rare Earth Resource Utilization of State Ethnic Affairs Commission, Key Laboratory of Photosensitive Materials and Devices of Liaoning Province, School of Physics and Materials Engineering, Dalian Minzu University, Dalian 116600, China
* Corresponding authors (emails: Ning.Liu@ul.ie (Liu N); dong@dlnu.edu.cn (Dong B))

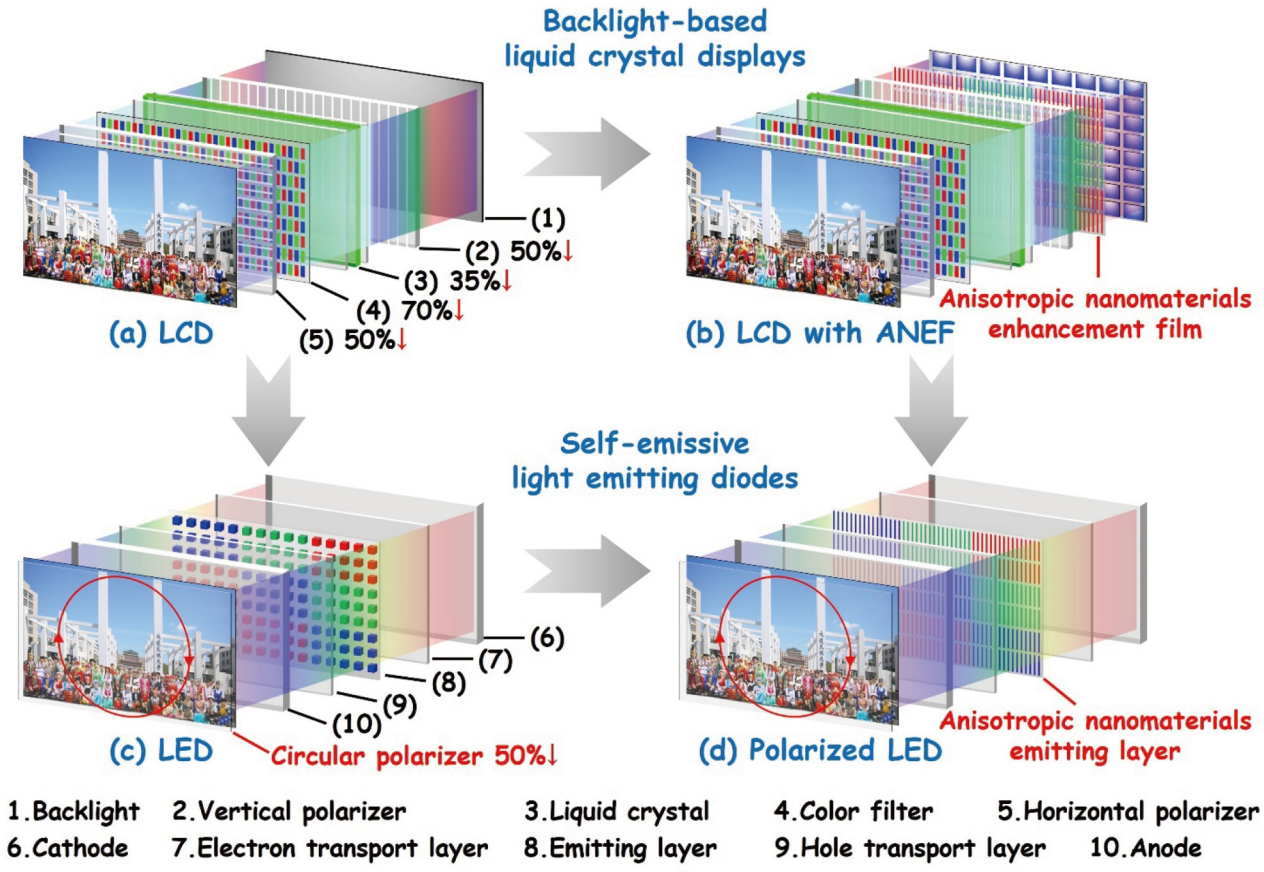

Scheme 1 The structure schematics of (a) traditional LCD system, (b) LCD system with ANEF, (c) QD LED, and (d) polarized QD LED.

can be obtained (Scheme 1b) [9,33]. The degree of polarization (DOP) is a very important parameter for nanomaterials and ANEF in practical application [34]. The direct cause of polarized light emission for nanomaterials is that their radiative transition dipole moments tend to be distributed along a certain direction [1,32,35–37]. Nanomaterials with anisotropic shapes usually exhibit higher DOP. This is because anisotropic nanomaterial can break the spherical symmetry, enabling polarized light emission along the long axis direction [7,26,38–40]. Based on above arguments, in order to obtain a high DOP in film emission, we need to use anisotropic nanomaterial emitters with high DOP, and align the anisotropic nanomaterials in a highly ordered and compact manner in a large area.

Different from backlight-based display technology in LCDs, the self-emissive QD LEDs are targeted to meet the demand of future display for high efficiency, high color purity, high resolution and wide color gamut (Scheme 1c) [41–46]. The external quantum efficiency (EQE) of red and green QD LEDs progressed significantly and achieved over 20% rapidly [43,44,47]. However, the metal electrodes in LEDs will reflect ambient light, which severely affects the display effect. Therefore, the circular polarizers are required to suppress ambient light reflection from the surroundings for high image contrast and outdoor visibility. Nevertheless, the use of circular polarizers loses more than 50% of the light energy from self-emissive QD LED. Fortunately, the construction of polarized LED could reduce energy loss, showing great promise in flexible displays and large-scale integration (Scheme 1d). Because the polarized LED based on orientation-aligned anisotropic nanomaterials can directly emit polarized light [9,48–52], when the polarized light is incident at a suitable angle relative to the main axis of the circular polarizer (0° or 90°), only a slight energy loss will be caused after passing through the circular polarizer. Though various approaches have been developed to arrange anisotropic nanomaterials into ordered patterns, the DOP and EQE of polarized LEDs are still limited due to the low DOP of films, the limitation of preparation methods, the poor quality of films and so on. Therefore, it is more desirable to look for effective aligning methods compatible with the standard LED fabrication process so as to fabricate polarized LEDs with high DOP and EQE.

Taking into account the potential importance of polarized light emission in future display market, a timely and thorough overview with the current literature related to polarized light emission is highly desirable. Therefore, in this review, we give a comprehensive summary on the state-of-the-art progress in the field of polarized light emission from materials to films, with a particular emphasis on polarized LEDs (Fig. 1). We begin with the theories of polarized light emission and analyze the factors that influence DOP. Sequentially, the polarized light emission properties from representative materials of QDs, NRs, NWs and NSs are described. Then, the assembly strategies for constructing polarized light emitting films and LEDs are summarized. Finally, we discuss the current challenges such as effective aligning methods compatible with the standard LED fabrication process, polarized light emission and charge carrier transport mechanisms for polarized LEDs, and give a brief conclusion and outlook

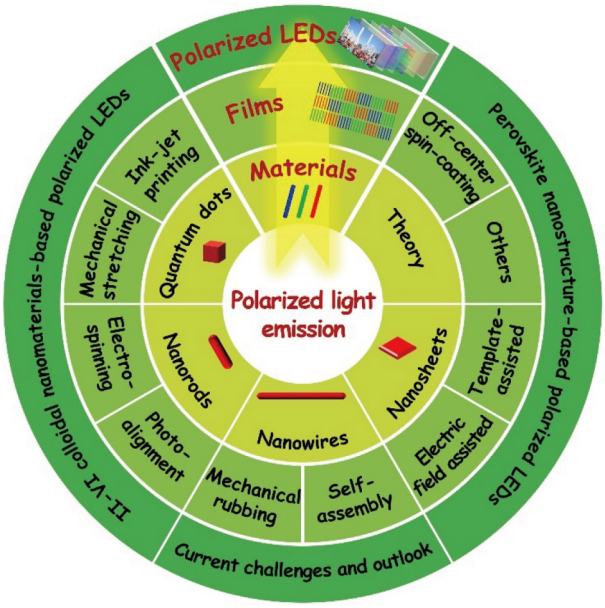

Figure 1 Schematic diagram of polarized light emission from different kinds of materials, films assembled by different methods and LEDs based on different nanomaterials.

on the potential commercial application prospect of the polarized LEDs. We hope this review would provide a valuable summary for current status of this research direction and stimulate some new insightful ideas for future development of this promising field.

POLARIZED LIGHT EMITTING MATERIALS

Polarization is a special physical property of light, which has significant application value not only in display, but also in imaging and information storage [53–56]. Some nanomaterials especially the anisotropic nanomaterials exhibit excitation and emission polarization [57,58]. To evaluate the effectiveness of polarized light emitting materials, some characterization definitions and mechanisms need to be quantified and well understood. In this section, the key parameters and influencing factors of polarized luminescence will be briefly introduced, and polarized light emission properties from QDs, NRs, NWs and NSs will also be summarized and compared.

Mechanism for linearly polarized light emission

The DOP (P) and anisotropy (R) value are important parameters used to measure the polarization ratio, which are defined as [34]

$$P = (I_{\parallel} - I_{\perp})/(I_{\parallel} + I_{\perp}), \quad (1)$$

$$R = (I_{\parallel} - I_{\perp})/(I_{\parallel} + 2I_{\perp}), \quad (2)$$

where $I_{\parallel}$ and $I_{\perp}$ are the light emission intensities parallel and perpendicular to the chosen alignment orientation, respectively. Normally, $I_{\parallel}$ is also the maximum intensity of the polarized light, and $I_{\perp}$ is the minimum. The value of P must be between 0 and 1, where $P = 0$ means that the material shows no polarized light emission. We pursue higher values of P for practical applications. When measuring the polarized light intensity, a rotatable linear polarizer needs to be placed between the material and the spectrometer in order to allow the polarized luminescence to pass through the polarizer. Then, the polarization angle-dependent luminescence signals can be obtained by the rotation of the polarizer periodically. And the DOP can be calculated *via* Equation (1). The size and morphology, in particular aspect ratio (AR) of the materials, are of vital importance to polarized light emission. It was reported that the nanomaterials with AR values more than 1.2 can realize partially polarized light emission [1,35,57,59–61].

In general, the polarized light emission is determined by anisotropic effective transition dipole moments, dielectric confinement of optical electric field, the splitting of the exciton fine structure and so on [32,35,62–68]. The polarized light emission mechanism for colloidal NRs is similar with that of core/shell colloidal NRs. Current polarized light emission mechanisms mainly focus on anisotropic core/shell colloidal nanomaterials [35].

For anisotropic 1D colloidal nanocrystals (NCs), their radiative transition dipole moments tend to be distributed along a certain axis, which is the direct cause of their polarized luminescence. Talapin *et al.* [64] demonstrated that efficient shape control may be achieved in the shell of colloidally grown semiconductor NCs, exhibiting high linearly polarized emission. The lowest excited state of wurtzite spherical NCs is generally an A-type exciton, which is optically forbidden along the c axis, whereas emission occurs from a higher B-type state with a transition dipole moment orthogonal to the c axis of the wurtzite structure. A non-spherical shape can lead to a swapping of the two states, with a strongly allowed dipole resulting in the direction of growth (c axis) due to the perturbation induced by the crystal field [64].

Another reason for linearly polarized luminescence of 1D colloidal NCs is the dielectric confinement effect. It originates from the difference in the dielectric constant of 1D colloidal NCs and the environment in which they are located. According to the theory of Wang *et al.* [65], when the lateral size of 1D nanomaterials is larger than 10 nm, since the size has exceeded the exciton Bohr radius of the same component bulk material, the quantum confinement effect will become weak. The classical electrodynamic theory can give a good explanation of the observed polarization anisotropy. The electric field strength in the 1D nanomaterial is determined by the dielectric constant of the 1D nanomaterial and the external environment, which can be expressed as

$$E_i = 2\varepsilon_0/(\varepsilon + \varepsilon_0) \times E_e, \quad (3)$$

where E_i is the electric field in the 1D nanomaterial, E_e is the excitation field, ε and ε_0 are the dielectric constants of the 1D nanomaterial and the external environment, respectively. According to the above expression, when the nanomaterial with a high dielectric constant is in an external environment with a low dielectric constant, if the incident field is polarized parallel to the nanomaterial, the electric field inside the nanomaterial will not reduce. But when polarized perpendicular to the nanomaterial, the electric field amplitude will attenuate [65].

The splitting of the exciton fine structure is another important reason for linearly polarized luminescence of 1D colloidal NCs. The spherical symmetry of the dot-like core should lead to a band-edge exciton structure with the same symmetry as for the spherical NCs, which show a low DOP for the emission. Vezzoli *et al.* [35] gave a detailed discussion on polarized emission and the fine structure of CdSe/CdS dot-in-rods made of a spherical core of CdSe surrounded by a rod-like shell of CdS. They presented a model of the polarized emission of CdSe/CdS dot-in-rods including the band-edge exciton fine structure, the shell anisotropy and the measurement configuration. They showed

that the DOP at room temperature was closely related to the fine structure. As can be seen in Fig. 2a, the valence band of CdSe consists of three sub-bands: the heavy hole band, light hole band and split-off band. The net-splitting Δ is the energy splitting at k = 0 of the heavy hole and light hole bands. The originally eightfold degenerate band-edge exciton ground state ($1S_{3/2}1S_e$) of CdSe NCs splits into eight fine structures of states $|\pm2\rangle$, $|\pm1^L\rangle$, $|\pm1^U\rangle$, $|0^L\rangle$, and $|0^U\rangle$ [36]. The superscripts L and U are used to distinguish the sublevels with same projection but different total angular momenta. As shown in the middle of Fig. 2a, the U states have higher energies than the L states. It has been shown that a level swapping of the fine structure appears for a certain AR of the CdSe NRs. It can be explained by the band structure of CdSe, where an inversion of the heavy hole and light hole sub-bands energy ordering at k = 0 implies a change in the fine structure level ordering.

The optically forbidden $|\pm2\rangle$states have no contribution to room-temperature emission. The $|0^L\rangle$ state is also optically inactive. Therefore, the room-temperature emission is mixed with recombination from the $|0^U\rangle$ state and from the degenerate $|\pm1^L\rangle$, $|\pm1^U\rangle$states [36]. The $|0^U\rangle$ state is related to a linear 1D dipole that oscillates along the c-axis of the crystal and emits linearly polarized photons. The $|\pm1^L\rangle$ and $|\pm1^U\rangle$ can be seen as 2D dipoles and they oscillate inside a plane. Because of the level degeneracy, the emission is an incoherent superposition of σ^+ and σ^- components, and the corresponding dipole is called a degenerate 2D dipole [69–71]. The two types of dipoles and the polarization of their far field emission are shown in Fig. 2b. These dipoles are contained in the plane perpendicular to the c-axis of the crystal, so the polarization azimuths for the two oscillators are mutually perpendicular. Therefore, the DOP for the total emission strongly depends on the relative oscillator strengths of two oscillators mutually oscillating in an orthogonal plane [1]. Fig. 2c presents the fine structure levels calculated for the DOP values of 0.38, 0.50 and 0.62.

Bai *et al.* [37] revealed the role of AR in the PL emission of single CdSe/CdS dot-in-rods using single-dot PL spectroscopy. They modeled the interrelation between DOP and AR by calculating the band-edge exciton fine structure. Fig. 2d shows the fine structure energy levels of CdSe/CdS dot-in-rods with different ARs. The $|\pm1^L\rangle$state contributes little to DOP, while the $|0^U\rangle$ and $|\pm1^U\rangle$ states contribute more significantly in determining the DOP. They found that when the AR reached 7, the contribution of the dielectric effect to the DOP became limited. The strain effect between the CdSe core and the CdS shell can change the ordering of the energy levels and the populations of emission states, thus increasing the DOP. Therefore, the DOP increased from 0.23 to 0.58 as the AR increased from 7.1 to 40.9.

With regard to perovskites, Yin *et al.* [72] studied bright exciton fine structure splitting in single perovskite $CsPbI_3$ NCs. Ramade *et al.* [73] investigated the fine structure of excitons and electron hole exchange energy in $CsPbBr_3$ single NCs. Folie *et al.* [74] studied the dynamics of band edge excitons in inorganic perovskite NWs. These studies proved that the polarized light emission from perovskites is also determined by the splitting of the exciton fine structure, anisotropic effective transition dipole moments, dielectric confinement of optical electric field and so on.

QDs

In general, compared with QDs, the anisotropic nanomaterials with larger AR values such as 1D NRs, 1D NWs and 2D NSs tend to have higher DOP [39,75]. However, the QDs can also emit polarized light in some cases. Wang *et al.* [39] synthesized

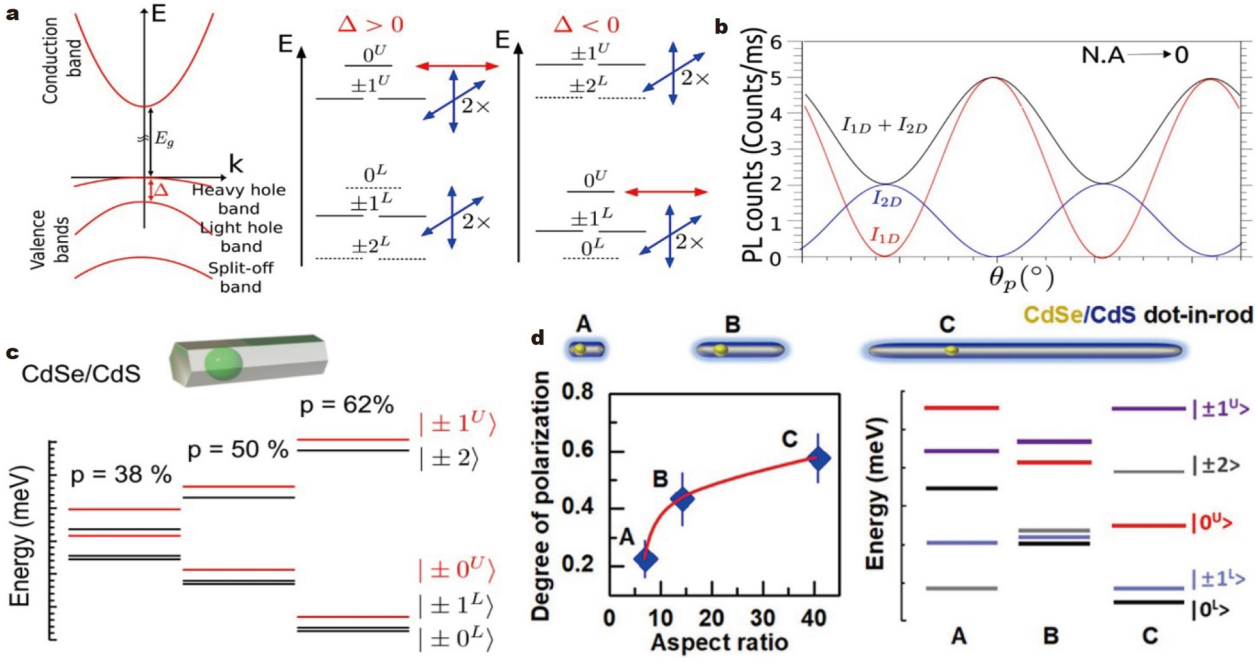

Figure 2 (a) Left: band structure of CdSe. Middle: band-edge exciton fine structure energy states for a positive net-splitting Δ. Right: band-edge exciton fine structure energy states for negative net-splitting Δ. (b) Schematics of a polarization measurement in the case of a numerical aperture close to 0. (c) Band edge exciton fine structures calculated for the DOP values of 0.38, 0.50 and 0.62. Reprinted with permission from Ref. [35], Copyright 2015, American Chemical Society. (d) Fine structure energy levels of CdSe/CdS dot-in-rods with different ARs. Reprinted with permission from Ref. [37], Copyright 2022, American Chemical Society.

$CsPb(Br_xI_{1-x})_3$ full inorganic perovskite QDs by changing the halide ratio and systematically studied polarized PL properties from these QDs for the first time. When x = 0, the DOP of $CsPbI_3$ was as high as 0.36 in solution and 0.40 as a film. Fig. 3a shows the experimental setup for polarized PL measurement. Fig. 3b, c show the polarization properties for $CsPbI_3$ and all the $CsPb(Br_xI_{1-x})_3$ QDs in hexane solution. The change of polarized emission intensity for $CsPbI_3$ QDs is consistent with the sine function. The DOP of $CsPb(Br_xI_{1-x})_3$ QDs improves with the increase of iodine amount. This may be due to the following two reasons. On one hand, the $CsPbBr_3$ perovskite belongs to the cubic crystal structure, while the $CsPbI_3$ perovskite is distorted cubic structure. The distorted cubic structure can break the space inversion symmetry and result in an asymmetrical structure, so as to enhance the polarization properties [40]. On the other hand, the $CsPb(Br_xI_{1-x})_3$ QDs are highly ionized, which facilitates self-organization forming of ordered packing structures in hexane. Shinde *et al.* [75] reported the structural distortions and polarized light emission from $CsPbBr_3$ nanocubes with different sizes, and indicated that smaller sized $CsPbBr_3$ nanocubes have higher polarized emission efficiency.

In addition to the full inorganic perovskite QDs, some organic-inorganic hybrid perovskite NCs also show polarized emission effects. The $MAPbI_3$ NCs exhibit a DOP of 0.28, which may be caused by the uniform alignment and distorted crystal structure of NCs [76]. Liu *et al.* [77] observed the linearly polarized emission in single $FAPbBr_3$ NCs at room and cryogenic temperatures. They speculated that the polarization phenomenon is attributed to the large energy-level splitting of the bright-exciton states, which leads to efficient exciton recombination from the lowest state with a 1D dipole moment.

The crystal structure of perovskite QDs can change in some solvents. Sun *et al.* [78] discovered that the polar solvent molecules can induce the phase transition of $CsPbI_3$ nanocubes from cubic to orthorhombic phase. Such lattice distortion also contributes to the hierarchical self-assembly of $CsPbI_3$ nanocubes into single-crystalline NWs. Besides, they revealed that more rapid self-assembly and phase transition processes can be induced by more amount or stronger polarity of solvents. Fig. 4a shows the schematic diagram of self-assembly process of $CsPbI_3$ from nanocubes to NWs. Although they did not investigate the polarized light emission properties, it was thought that the DOP of NWs was improved because of the asymmetrical structure.

The polarization anisotropy can also be achieved in dimers of two laterally coupled QDs, because the separate excitons in the two QDs can be coupled through the dipole–dipole interaction. Kim *et al.* [79] studied the polarization anisotropy in a dimer of laterally coupled GaAs QDs and found that the emission from laterally coupled QDs is strongly polarized along the coupled direction. As can be seen in Fig. 4b, c, a DOP of 74% can be observed when the excitation polarization is parallel to the coupled direction, while it is only 10% when the excitation polarization is perpendicular to the coupled direction. At last, they proved that the dipole–dipole interaction across two separate QDs is mediated. The anisotropic wavefunctions are determined by the excitation polarization.

NRs

NRs exhibit stronger polarized light emission property over QDs because of their higher anisotropy [37,80–82]. Colloidal semiconductor NRs are important polarized light emitting materials researched most early, including NRs, dot-in-rod and rod-in-rod core/shell nanostructures [26,83–85]. In 2001, Hu *et al.* [57] studied linearly polarized emission of CdSe colloidal NCs. Through empirical pseudopotential calculations, they predicted that different from plane-polarized light for spherical dots, the slightly elongated CdSe NCs can emit polarized light along the long axis. They also confirmed that there is a sharp transition from nonpolarized to purely linearly polarized emission at the AR of 2 by single-molecule luminescence spectroscopy mea-

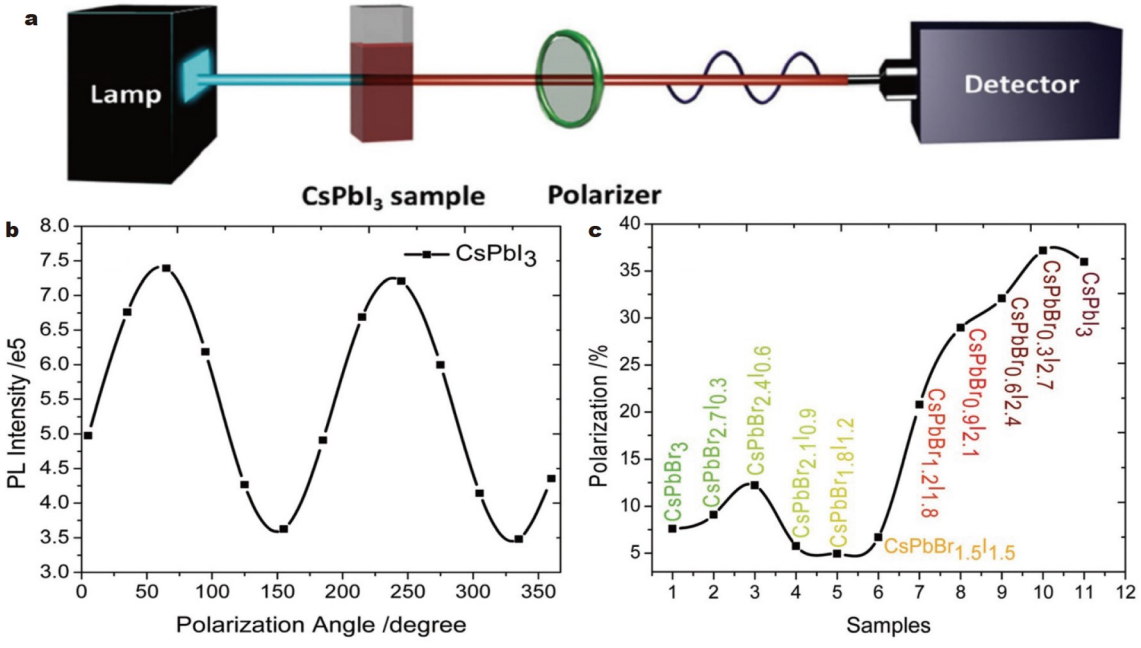

Figure 3 (a) Experimental setup for the polarized PL measurement. (b) Polarization property for $CsPbI_3$ QDs in hexane solution. (c) Polarization properties for all the $CsPb(Br_xI_{1-x})_3$ QDs in hexane solution. Reprinted with permission from Ref. [39], Copyright 2016, The Royal Society of Chemistry.

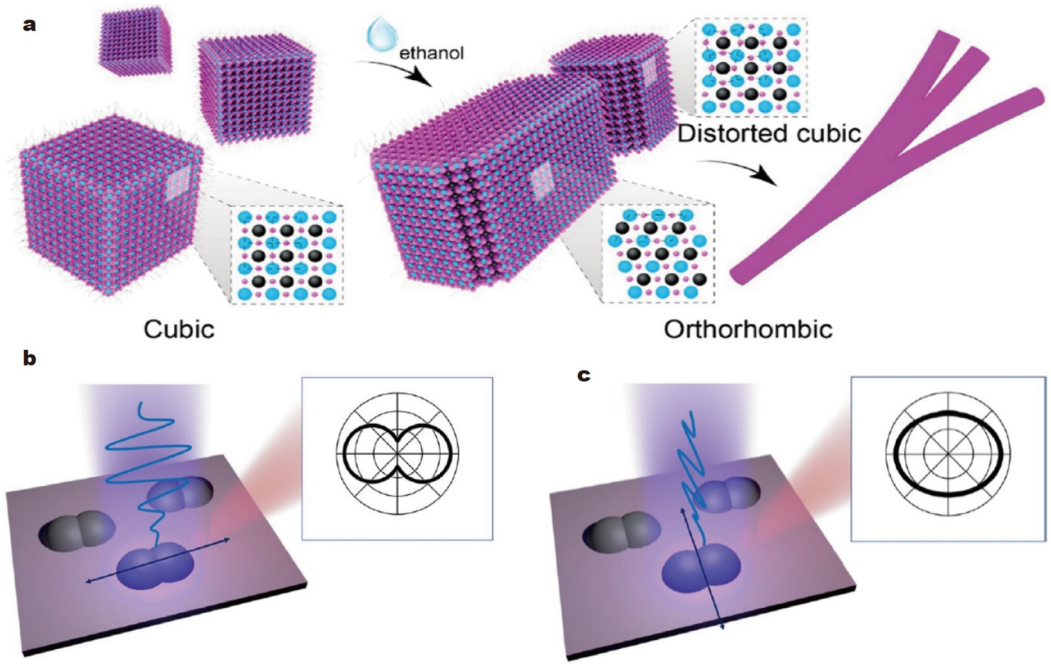

Figure 4 (a) Schematic diagram of the self-assembly process of $CsPbI_3$ from nanocubes to NWs. Reproduced with permission from Ref. [78], Copyright 2018, American Chemical Society. The polarization anisotropy in a dimer of laterally coupled GaAs QDs when the excitation polarization is (b) parallel and (c) perpendicular to the coupled direction. Reprinted with permission from Ref. [79], Copyright 2020, Nature Publishing Group.

surements. Since then, polarized light emission optimization from length-diameter ratio AR adjustment, structure optimization, surface modification and doping regulation has developed rapidly in the following years.

Carbone *et al.* [86] reported a seeded-growth method to synthesize CdSe/CdS dot-in-rod core-shell NRs with asymmetric structure, regular morphology, narrow distribution of size and linearly polarized emission. More importantly, the AR could be adjusted easily through simply changing the dosage of the precursor and reaction temperature. They also achieved the lateral and vertical alignments of CdSe/CdS NRs on the substrates up to micrometer-size. Fig. 5a shows the schematic diagram of the seeded growth method. Fig. 5b–f show the transmission electron microscopy (TEM) images of CdSe/CdS NRs with different sizes. Sitt *et al.* [87] synthesized CdSe/CdS rod-in-rod core/shell NRs by the seeded-growth method. The NRs exhibited uniform size, high emission quantum efficiencies and highly polarized emission. They found the DOP was controlled by the inner core rod dimensions. They also measured the polarization property at different excitation wavelengths and studied the interaction between electronic contribution and dielectric effect in determining the absorption and emission polarization. Fig. 5g, h show the parallel and perpendicular polarized emissions of core/shell and rod-in-rod CdSe/CdS nanostructures, respectively. As can be seen, the rod-in-rod CdSe/CdS nanostructure shows much higher difference between the polarization components, the DOP is calculated to be 0.37. Instead of CdSe/CdS heterostructure, Hadar *et al.* [88] synthesized CdSe/$Cd_{1-x}Zn_xS$ NRs with high green emission quantum yield and high polarization through controlled addition of Zn atoms (Fig. 5i).

Metal halide perovskite NRs are emerging as materials with prominent optical and electronic properties, which can also offer the remarkable property of linearly polarized light emission [89]. Li *et al.* [89] realized the direct synthesis of two kinds of $CsPbBr_3$ NRs in polar alcohols with the average lengths of 10.8 and 23.2 nm. The PLQY of 76% is realized in the short $CsPbBr_3$ NRs. As can be seen in Fig. 6a, the $CsPbCl_3$ and $CsPbI_3$ NRs can be easily synthesized by anion-exchange reactions, and the emission can vary across the full visible wavelength range. TEM images provided in Fig. 6b confirm the NR shape of the pristine $CsPbCl_3$, $CsPbBr_3$ and $CsPbI_3$ NRs with similar size. Fig. 6c shows the different PL intensities of long $CsPbBr_3$ NRs measured in two different polarizer directions. Fig. 6d compares the *R* values of $CsPbBr_3$ NCs, short NRs and long NRs. Among them, the $CsPbBr_3$ NCs presented a featureless emission polarization spectrum; and the long $CsPbBr_3$ NRs showed the highest anisotropy because of their highest length-diameter ratio. Dou *et al.* [30] realized an enhanced *R* value in the $CsPbBr_{1.2}I_{1.8}$ NRs compared with pristine $CsPbBr_3$ NRs. because the substitution of smaller bromine anions with larger iodine anions can induce structural distortion of PbX_6 octahedra units and so as to break the lattice symmetry. As can be seen from the PL anisotropy curves shown in Fig. 6e, the $CsPbBr_{1.2}I_{1.8}$ NRs show the PL *R* value around 0.4, which is four-fold higher than that of pristine $CsPbBr_3$ NRs. Zhao *et al.* [90] found the PL intensity and radiative lifetime are sensitive to the polarization direction. As can be seen in Fig. 6f, the PL of $CsPbBr_3$ NRs shows clear changes in intensity, with the strongest intensity in parallel and the weakest in vertical directions to the NRs, while the PL from $CsPbBr_3$ NCs remains unchanged with the different polarization angles. Moreover, they found that the radiative lifetimes of $CsPbBr_3$ NRs are affected by different excitation polarization angles (Fig. 6g). Except the inorganic halide perovskite NRs, the rod-like aggregates $MAPbBr_3$ QDs also show different emission intensities in the parallel and perpendicular to the rod-like packing directions (Fig. 6h) [91].

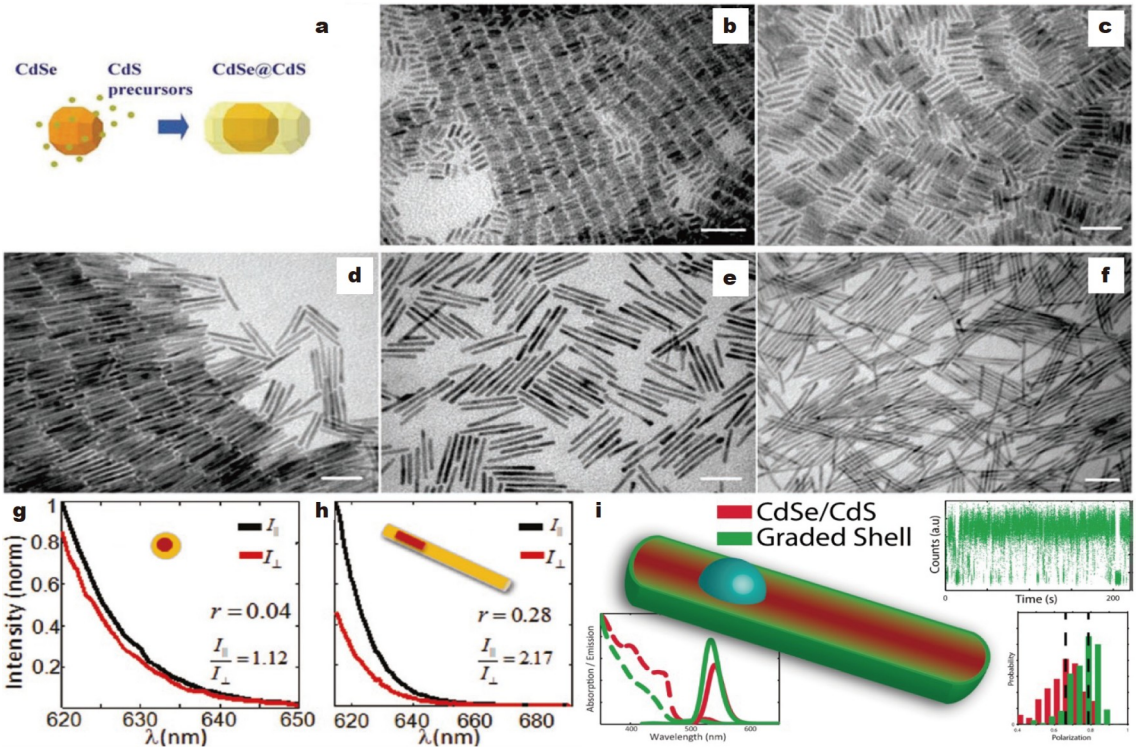

Figure 5 (a) Schematic diagram of the seeded growth method. (b–f) TEM images of CdSe/CdS NRs with different sizes. All scale bars are 50 nm. Reprinted with permission from Ref. [86], Copyright 2007, American Chemical Society. The parallel and perpendicular polarized emissions of (g) core/shell and (h) rod-in-rod CdSe/CdS nanostructures. Reprinted with permission from Ref. [87], Copyright 2011, American Chemical Society. (i) Absorption (dashed), emission (solid) spectra and emission polarization distributions of NRs. Reprinted with permission from Ref. [88], Copyright 2017, American Chemical Society.

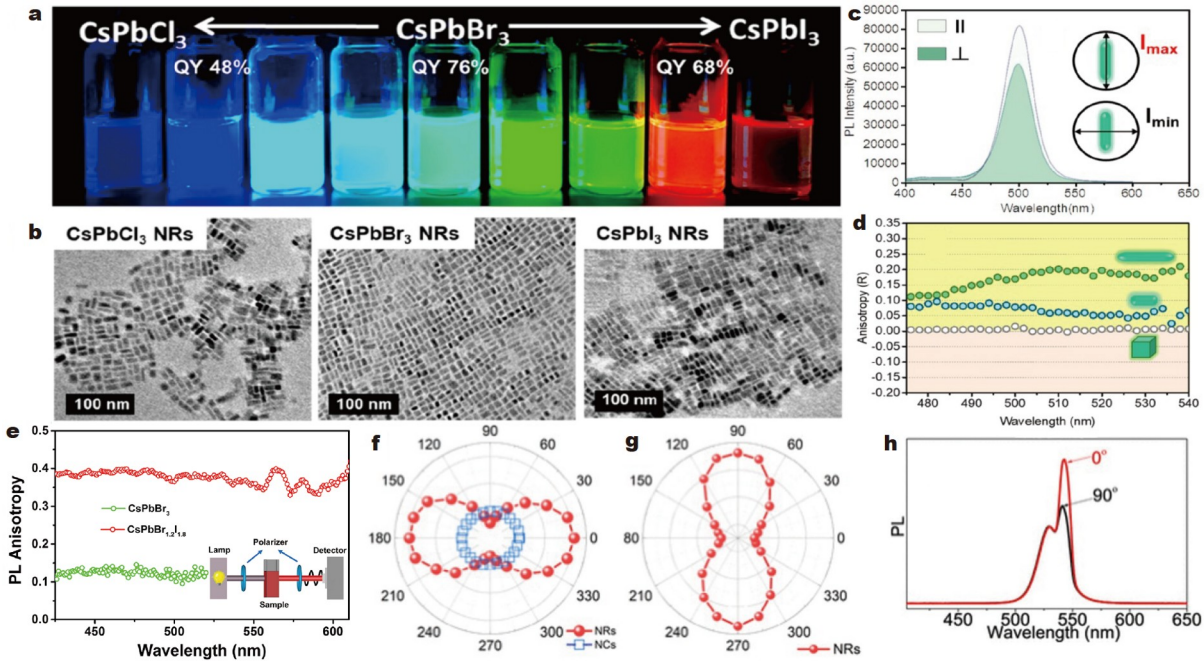

Figure 6 (a) Photograph of $CsPbX_3$ NR solutions under 365-nm ultraviolet (UV) lamp irradiation. (b) TEM images of the pristine $CsPbCl_3$, $CsPbBr_3$ and $CsPbI_3$ NRs with similar size. (c) Different PL intensities of long $CsPbBr_3$ NRs measured in two orthogonal polarizer directions. (d) *R* values of the $CsPbBr_3$ NCs, short NRs and long NRs at different wavelengths of emission. Reprinted with permission from Ref. [89], Copyright 2019, American Chemical Society. (e) PL *R* curves of $CsPbBr_3$ and $CsPbBr_{1.2}I_{1.8}$ NRs. Reprinted with permission from Ref. [30], Copyright 2020, American Chemical Society. (f) PL intensity *versus* excitation polarization of $CsPbBr_3$ NRs and NCs. (g) Lifetime *versus* excitation polarization of $CsPbBr_3$ NRs. Reprinted with permission from Ref. [90], Copyright 2022, American Chemical Society. (h) Lifetime *versus* excitation polarization of $CsPbBr_3$ NRs. Reprinted with permission from Ref. [91], Copyright 2021, American Chemical Society.

NWs

Compared with QDs and NRs, the NWs possess inherently larger AR, giving them a competitive advantage in anisotropy and polarized light emission [65,92–98]. Colloidal semiconductor NWs are therefore attractive materials with strong polarized light absorption and emission. Yang *et al.* [93] synthesized ultralong colloidal $CdSe_xS_{1-x}$ NWs through a solution-liquid-solid method. The optical band and PL spectra of $CdSe_xS_{1-x}$ NWs can be finely tuned from 508 to 628 nm by varying the ratio of Se/S. More importantly, the $CdSe_xS_{1-x}$ networks show strong polarized emission with DOP up to 0.6, which is much higher than that of the CdSe/CdS dot-in-rod or rod-in-rod samples. It is also feasible to detect polarized light by colloidal NWs. Yu *et al.* [99] synthesized randomly oriented CdSe NW networks for photocurrent measurements. They proved that the photocurrent is sensitive to the orientation between the incident polarized light and the external applied electric field, and the maximum photocurrent occurs when the light polarization is parallel to the electric field direction.

There are also many studies exploring the synthesis methods of lead halide perovskite NWs. Yang's group [94,95] made a lot of efforts in this regard. They reported a catalyst-free, solution-phase method to synthesize $CsPbX_3$ single-crystalline NWs with uniform diameter that crystallize in the orthorhombic phase [94]. Afterwards, they used highly monodisperse $CsPbBr_3$ NWs as the templates to synthesize $CsPb(Br/X)_3$ (X = Cl, I) NWs [95]. The prepared alloy NWs have well-preserved morphology and crystal structure. As shown in Fig. 7a, the NWs with a wide range of alloy compositions can emit bright PL over almost the entire visible spectrum. Then, they successfully synthesized and purified highly uniform single crystal ultrathin $CsPbBr_3$ NWs through a catalyst-free colloidal synthesis followed by a stepwise purification method [100]. After surface treatment, the ultrathin $CsPbBr_3$ NWs with a diameter of 2.2 nm and length up to several microns have bright PL, and the PLQY can be up to about 30%. Gao *et al.* [101] synthesized the well-aligned $CsPbBr_3$ and $CsPbCl_3$ NWs with thicknesses of 15 and 7 nm using a vapor phase van der Waals epitaxial method. They demonstrated the NWs with thicknesses less than 40 nm have strong emission anisotropy with DOP up to 0.78 due to the electrostatic dielectric confinement. Fig. 7b compares the polarization dependence of integrated PL intensity as a function of polarization angle. The NWs of 15 nm thick have obviously higher anisotropy than that of 250-nm-thick NWs. As shown in Fig. 7c, the PL images of the NWs under different excitation polarization angles are also in accord with the PL intensity. Zhou *et al.* [102] developed flexible linearly polarized photodetectors based on $CsPbI_3$ NWs. Because of the excellent crystal structure and morphology anisotropy of $CsPbI_3$ NWs, the polarized photodetector is highly sensitive to the polarization direction of light. The flexible device shown in Fig. 7d has high flexibility, transparency and polarization-dependent photocurrent response.

NSs

2D NSs exhibit exceptional photophysical properties, for example, increased exciton binding energy, low threshold sti-

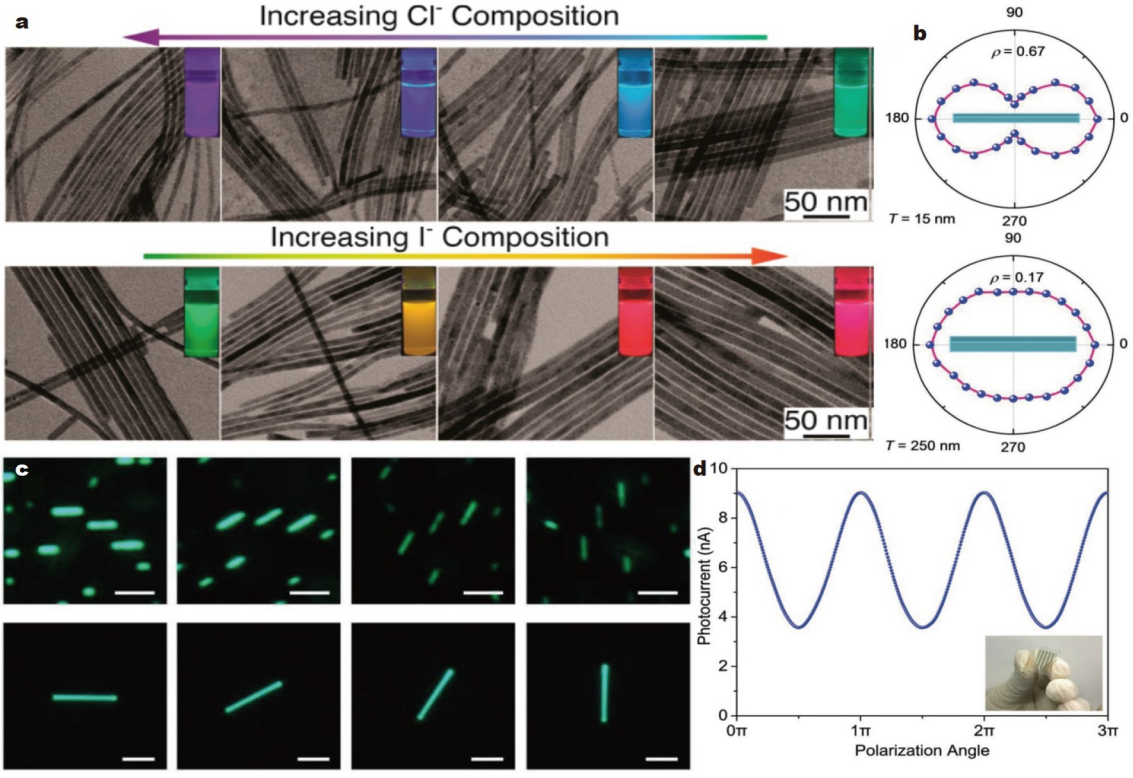

Figure 7 (a) TEM images of $CsPbX_3$ NWs. Reprinted with permission from Ref. [95], Copyright 2016, American Chemical Society. (b) PL intensity of $CsPbBr_3$ NWs as a function of excitation polarization. (c) Optical PL images at different polarization angles (0°, 30°, 60° and 90° from left to right). Scale bars for upper and lower four images are 250 nm and 3 μm, respectively. Reprinted with permission from Ref. [101], Copyright 2018, Wiley-VCH Verlag GmbH & Co. KGaA, Weinheim. (d) Polarization-dependent photocurrent of the flexible photodetectors based on $CsPbI_3$ NWs. Reprinted with permission from Ref. [102], Copyright 2018, Wiley-VCH Verlag GmbH & Co. KGaA, Weinheim.

mulated emission, enhanced absorption cross-section with respect to bulk, and remarkable optical nonlinearities. However, they are more difficult to align [103–109].

Cassette *et al.* [108] reported the synthesis and properties of novel 2D CdSe/CdS dot-in-plate NCs with polarized emission. The NCs were synthesized by growing the disciform CdS shell on spherical CdSe cores. Fig. 8a, b show the CdSe/CdS dot-in-plate NCs lying flat or standing on their edges. The CdSe/CdS dot-in-plate NCs exhibit strong polarized emission in the plane perpendicular to the wurtzite crystal *c* axis (Fig. 8c). Fig. 8d shows the schematic of energy levels and the orientation of the corresponding transition polarizations with respect to the crystallographic structure in CdSe/CdS dot-in-plate NCs. The energy levels and oscillator strengths of the optically active ones, the $|0^U\rangle$, $|\pm1^U\rangle$, and $|\pm1^L\rangle$states, control the emission properties, especially the polarization. The $|0^U\rangle$transition is linearly polarized along the *c* axis (π transition) [108]. Controlling the orientation of a single fluorescent nanoparticle in a desired orientation and measuring their emission spectra are still a big challenge. Feng *et al.* [110] proved the single cubic CdSe/CdS NSs have different fluorescence dipoles in vertical and horizontal orientations. As can be seen in Fig. 8e, the cubic-shaped CdSe/CdS NSs are structured with a thin CdSe core layer sandwiched in a thick CdS shell. Fig. 8f compares the polarization analysis curves for two typical NSs, where the DOP for the horizontal NSs is very close to 0, while the vertical NSs exhibit a much higher DOP of 0.79. Besides, the measurements and calculations show a good agreement in 2D dipole orientation (Fig. 8g). Ma *et al.* [111] reported anisotropic PL from isotropic optical transition dipoles in semiconductor NSs. Feng *et al.* [112] demonstrated that the emission is polarized and the emission patterns are anisotropic for rectangular NSs; while they showed non-polarized and isotropic properties for square NSs.

Recently, perovskite crystals also play an important role in 2D NSs. Bekenstein *et al.* [104] reported highly luminescent perovskite cesium lead halide colloidal NSs. They observed that the reaction temperature is vitally important for the shape and thickness of $CsPbBr_3$ NCs. As can be seen in Fig. 9a–c, reactions conducted at 150, 130, and 90°C produce NCs, NSs and thin NSs, respectively. They also have different-color PL emission. Sheng *et al.* [113] synthesized all-inorganic $CsPbX_3$ perovskite 2D NSs. They have uniform thickness and tunable size, and they can be easily controlled by changing the component and amount of metal halides, temperature, time, and ligands. Fig. 9d shows that differently shaped perovskite NCs can be obtained by changing the dosage of $CuCl_2$. Zeng *et al.* [114] synthesized $CsPbBr_3$ NSs with a PLQY of 97.4% using the aged Pb-oleate precursor. Fig. 9e shows the diagrams and TEM images of fresh-precursor sample (top) and aged-precursor sample (bottom).

Liu *et al.* [115] synthesized the $CH_3NH_3PbBr_3$ NSs through a self-organization method. The spherical nanodots will transform to square or rectangular NSs when the colloidal NCs are kept at a high concentration for three days, or the synthesis of nanodots is combined with self-organization. Additionally, after being

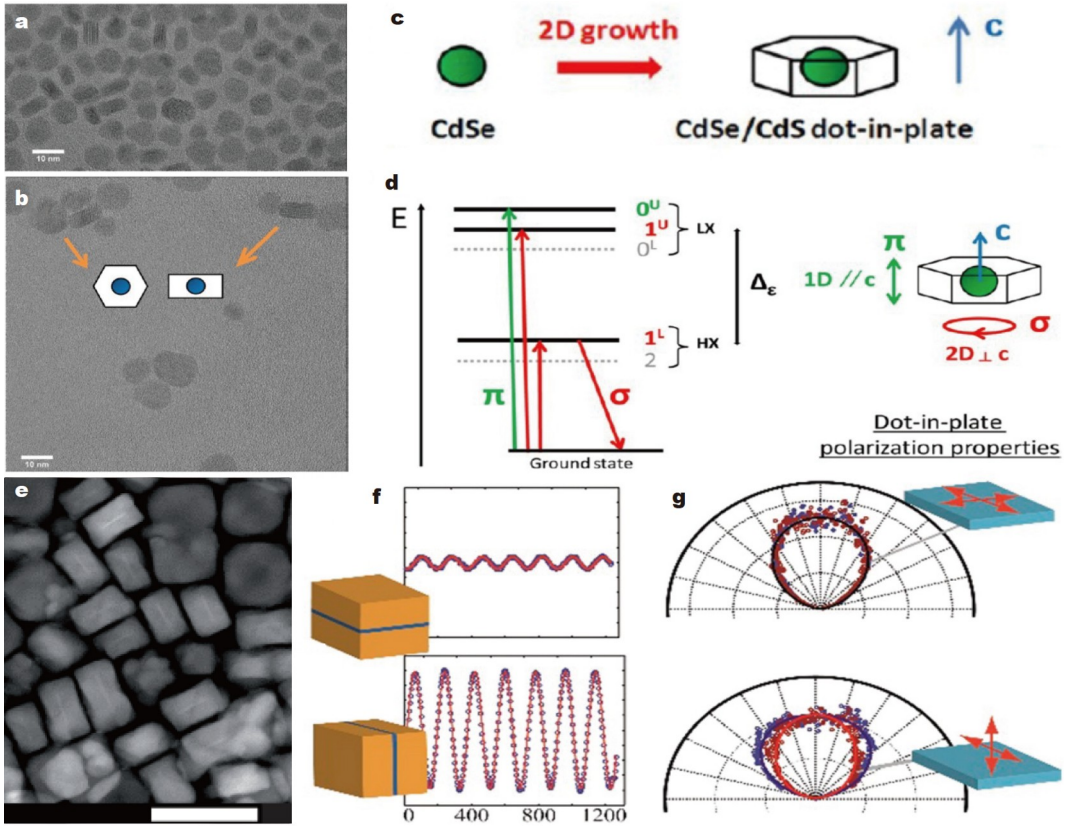

Figure 8 TEM images of CdSe/CdS dot-in-plate NCs of 4 (a) and 6 (b) equivalent CdS monolayers. (c) Schematic for CdSe/CdS dot-in-plate NCs with strong polarized emission in the plane perpendicular to the wurtzite crystal *c* axis. (d) Schematic of energy levels and the orientation of the corresponding transition polarizations with respect to the crystallographic structure. Reprinted with permission from Ref. [108], Copyright 2012, American Chemical Society. (e) TEM image of the CdSe/CdS NSs (scale bar: 50 nm). (f) Polarization analysis curve for two typical NSs. (g) Experimental measurements and calculations of the 2D dipole. Reprinted with permission from Ref. [110], Copyright 2018, American Chemical Society.

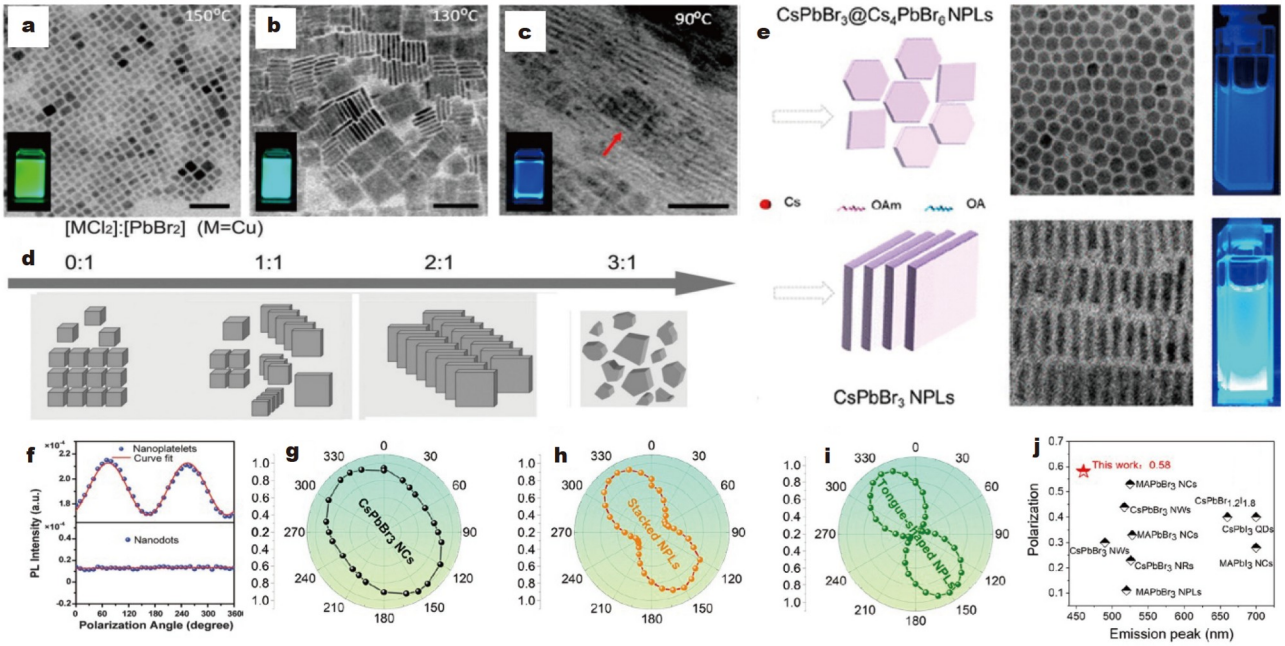

Figure 9 TEM images of (a) NCs, (b) NSs and (c) thin NSs synthesized at 150, 130 and 90°C, respectively. All scale bars are 50 nm. Reprinted with permission from Ref. [104], Copyright 2015, American Chemical Society. (d) Schematic of different shaped perovskite NCs controlled by different dosages of $CuCl_2$. Reprinted with permission from Ref. [113], Copyright 2018, Wiley-VCH Verlag GmbH & Co. KGaA, Weinheim. (e) Diagrams and TEM images of $CsPbBr_3$ NSs synthesized by the fresh-precursor sample (top) and aged-precursor sample (bottom). Reprinted with permission from Ref. [114], Copyright 2021, American Chemical Society. (f) PL intensity of the stretched $CH_3NH_3PbBr_3$ NS film as a function of polarizer angle. Reprinted with permission from Ref. [115], Copyright 2017, Wiley-VCH Verlag GmbH & Co. KGaA, Weinheim. Integrated PL intensities as a function of polarization angles for the samples of (g) $CsPbBr_3$ NCs, (h) stacked shaped NSs and (i) tongue-shaped NSs, respectively. (j) Comparison of polarization effect for different perovskite nanomaterials. Reprinted with permission from Ref. [116], Copyright 2022, Springer Nature.

stretched for 2–3 times, the polymer composite film embedded with $CH_3NH_3PbBr_3$ NSs exhibits expected polarized emissions, and the DOP is 0.11. As can be seen in Fig. 9f, the PL emission of stretched film shows the cos/sin intensity dependence on the polarization angles. Yang *et al.* [116] proposed a two-step nucleation strategy to synthesize $CsPbBr_3$ NSs. Subsequently, they prepared the $CsPbBr_3$ NS films by a dip coating method for the polarization measurement. Fig. 9g–i show the integrated PL intensities as a function of polarization angles for the samples of $CsPbBr_3$ NCs, stacked shaped NSs and tongue-shaped NSs, respectively. Fig. 9j compares the polarization effect of different perovskite nanomaterials, where the DOP of 0.58 for $CsPbBr_3$ NS film is relatively high.

In addition to the above-mentioned polarized light emission materials, the tetrapod-shaped, bone-shaped and some other anisotropic heterostructures may also have the potential for polarized light emission with high DOP [117,118].

FABRICATION OF LINEARLY POLARIZED LIGHT EMITTING FILMS

It is expected that the aligned ANEF with large size, good uniformity and densification would emit polarized light with high DOP, so as to further enhance the efficiency of LCD and benefit the fabrication of polarized LEDs [9,18,32,119]. Since the alignment of anisotropic nanomaterials is vitally important, many techniques have been explored to obtain high-quality ANEFs recently, including ink-jet printing, mechanical stretching, electrospinning, photoalignment, mechanical rubbing, self-assembly at the liquid/air interface, electric field-assisted assembly, template-assisted assembly, and off-center spin-coating. Several other less significant methods have also been investigated. Most of these methods need the assistance of external force, therefore limiting the flexibility and local alignment orientation to a certain extent. And most importantly, some methods are inapplicable to the fabrication of LEDs. In this section, we would summarize and compare the different methods to construct polarized light emitting films.

Ink-jet printing

The non-contact ink-jet printing technique offers a possibility to achieve uniform, well-aligned and large-scaled polarized light emitting films. This method would have a broad application prospect in polarized optoelectronic devices, LCD backlights and some other fields where polarized light is needed. The year of 2019 was a boom year to align semiconductor and perovskite nanomaterials by ink-jet printing. Gupta *et al.* [120] demonstrated that the ink composition and printing conditions have a great influence on the alignment quality of CdSe/CdS rods. Their ANEFs show a DOP of 0.76. When combining ANEFs with blue LED as the backlight display unit for LCD, the system provides an unprecedented increase of optical efficiency for 77% and simultaneously offers better color space. Fig. 10a shows the schematic of the ANEF printing process followed by photopolymerization under UV light. Fig. 10b gives the schematics of different flow processes in the ink-jet printing films. The color triangle of the LCD shown in Fig. 10c covers 109% of NTSC on the CIE1976 color triangle.

Zhou *et al.* [38] made a great contribution for the practical application of ink-jet printing. Using this method, they produced many devices by 3D-printed nanocomposite inks com-

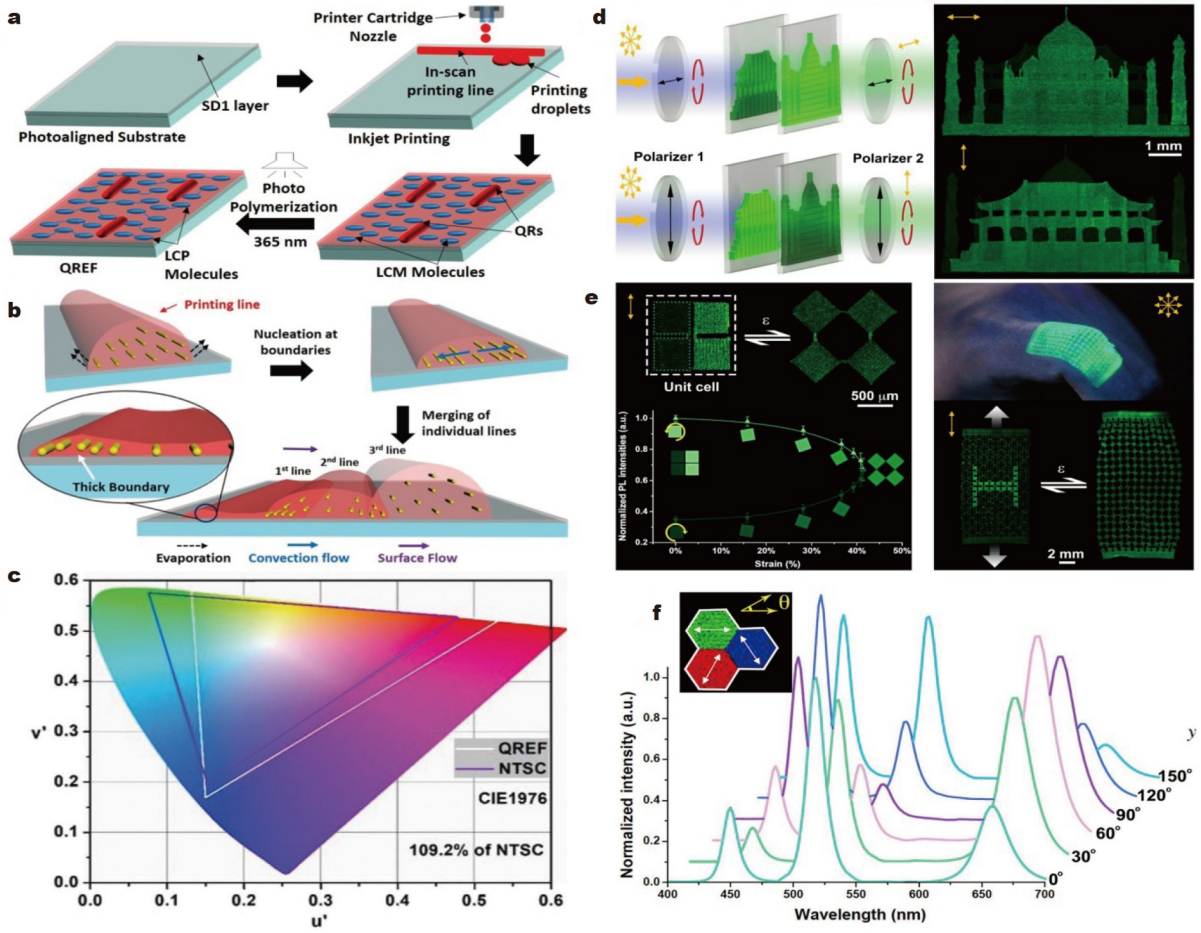

Figure 10 (a) Schematic illustration of the ANEF printing process followed by photo-polymerization under UV light. (b) Schematics of the different flow processes in the ink-jet printing films. (c) CIE1976 color triangle for the ANEF-based backlight unit. Reprinted with permission from Ref. [120], Copyright 2019, The Royal Society of Chemistry. (d) Polarization holograms. (e) A mechano-optical metamaterial based on an auxetic structure. (f) Spectral emissions of the pixel array based on hexagonal tiles of red, green and blue perovskite nanomaterials printed along three directions. Reprinted with permission from Ref. [38], Copyright 2019, American Association for the Advancement of Science.

posed of perovskite NWs and block copolymer matrix, such as optical storage, encryption, sensing, and full-color displays. These devices have high polarized absorption and emission properties. Fig. 10d, e show the applications of ink-jet printing for security encryption and optical strain sensors. Fig. 10f presents the spectral emission profiles of the pixel array based on hexagonal tiles of red, green, and blue perovskite nanomaterials printed along three directions. Zhou *et al.* [121] aligned the CdSe/CdS core/shell quantum rods by the contact ink-jet printing method. When printing the ink, the quantum rods will align along the fluid ink flow direction, resulting in aligned quantum rods and forming a polarized light emission film with a DOP of 0.42.

Mechanical stretching

Mechanical stretching is a simple and common method for arranging nanomaterials, which is suitable for producing large-area-polarized light source [9,32,119,122–124]. During the stretching process, the nanomaterials are rotated and aligned along the stretching direction by the shear stress provided by the polymer segment. This method requires that the nanomaterials have good compatibility with the selected polymer, and the polymer can also protect the nanomaterials from the environment. Besides, the polymer needs to have a large stretching ratio so that the nanomaterial film could have a large degree of orientation.

Cunningham *et al.* [9] obtained semiconductor-polymer polarized light emission composite films by this method. The films with high DOP of 0.7 are viable candidates for practical application in LCD devices. Compared with the emitter layers with randomly oriented CdSe/CdS nanomaterials, the composite films with aligned CdSe/CdS nanomaterials exhibit more than two times enhancement of brightness. Fig. 11a presents the composite films under UV light before and after stretching. Fig. 11b shows the polarized PL dependence from the composite films before (squares) and after (circles) stretching. The DOP of stretched films is 0.6, while it is only about 0.05 for the non-stretched films. Raja *et al.* [123] demonstrated enhanced water and light stability of colloidal perovskite nanomaterials by encapsulating them into polymeric matrices. Fig. 11c, d show the images of aligned perovskite NWs and polymer composite film observed by optical microscope and confocal microscope, respectively. As can be seen in Fig. 11e, the DOP of the aligned NWs polymer composite is about 0.44, which is more than five

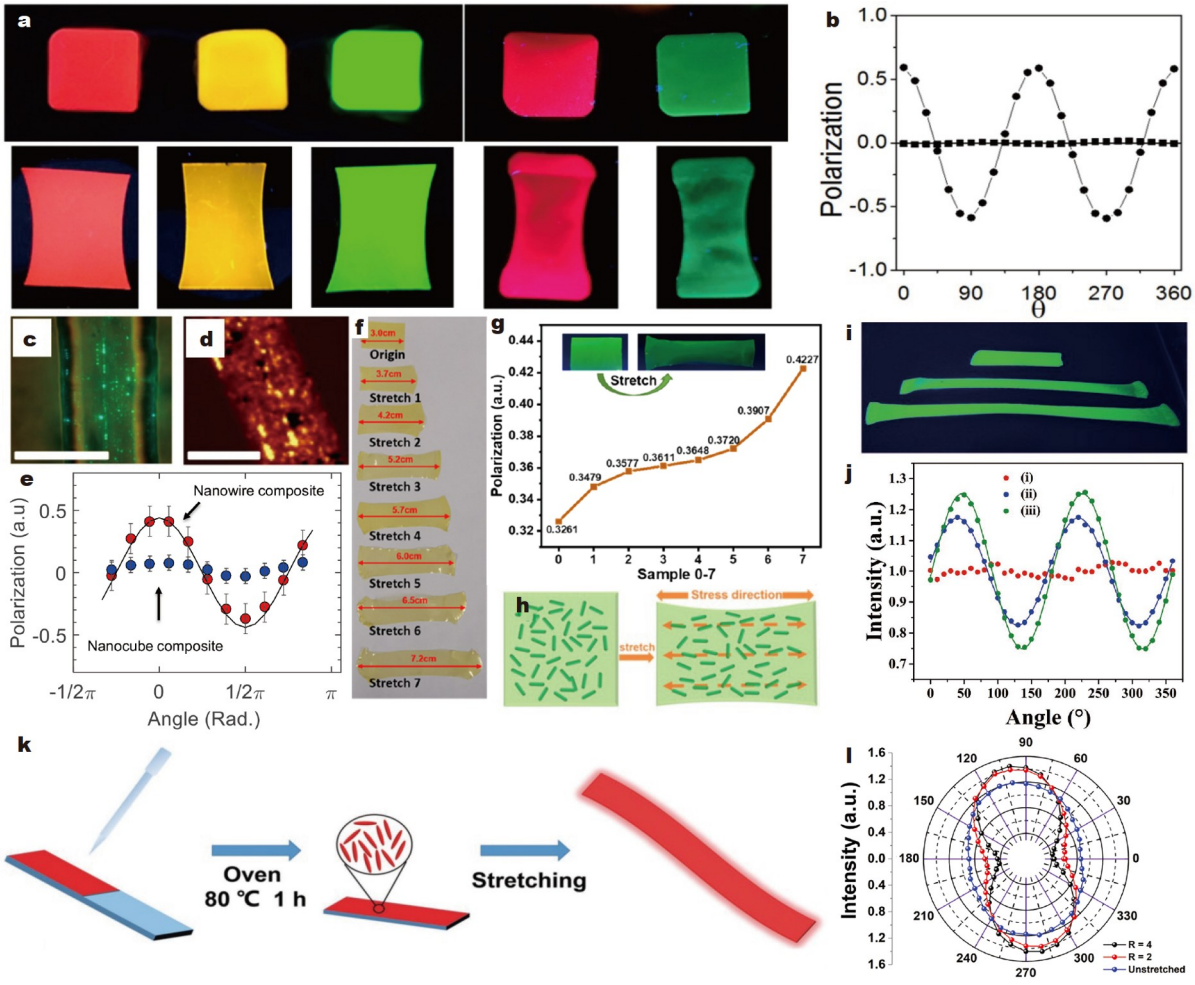

Figure 11 (a) Semiconductor-polymer polarized light emission composite films under UV light before and after stretching. (b) Polarized PL dependence of composite films before (squares) and after (circles) stretching. Reprinted with permission from Ref. [9], Copyright 2016, American Chemical Society. Images of aligned perovskite NWs and polymer composite film observed by (c) optical microscope and (d) confocal microscope, respectively (scale bars are 20 μm). (e) DOP as a function of polarized angle of NWs polymer fiber (red) and NCs polymer fiber (blue). Reprinted with permission from Ref. [123], Copyright 2016, American Chemical Society. (f) Photographs of unstretched perovskite NWs-PMMA composite film and other seven samples with different stretched lengths. (g) DOP of eight different films. (h) Schematic diagram of mechanical stretching improving polarization. Reprinted with permission from Ref. [124], Copyright 2021, American Chemical Society. (i) Photograph of perovskite-NC-embedded polymer composite film under UV irradiation. (j) PL intensities of the films before and after stretching as a function of polarizer angle. Reprinted with permission from Ref. [32], Copyright 2017, Wiley-VCH Verlag GmbH & Co. KGaA, Weinheim. (k) Schematic diagram of the construction of the CdSe@CdS/PVDF composite films. (l) Angle-dependent emissions of the composite films before and after stretching. Reprinted with permission from Ref. [119], Copyright 2019, Wiley-VCH Verlag GmbH & Co. KGaA, Weinheim.

times higher than that of NCs.

Wang *et al.* [124] synthesized $CsPbBr_3$ NWs and polymethyl methacrylate (PMMA) polymer composite films with strong polarized PL. The optimized stretched composite film can achieve a DOP of 0.42. Then, they used the film as a fluorescence conversion layer to enhance the UV polarization light detection. Their results demonstrated that the response is greatly enhanced after spectral conversion, and different responsivities correspond to different polarization states. Fig. 11f shows the images of unstretched film and other seven samples with different stretched lengths. Fig. 11g shows the polarization curve of different samples. After stretching, the DOP of the film is improved significantly. Fig. 11h explains the reason of improved polarization through mechanical stretching. Under the stretching force, the $CsPbBr_3$ NWs in the PMMA polymer film would deflect in the stretching direction.

Zhong's group [32,119] carried out a series of work by this method. Lu *et al.* [32] reported strong polarized PL from stretched perovskite nanomaterials and polymer composite films. The perovskite QDs in the composite films would be aligned into wires and emit polarized light with a DOP up to 0.33. Fig. 11i shows the photograph of films under UV irradiation. As can be seen from the polarization measurements of composite films in Fig. 11j, the composite films exhibit non-polarized emission before stretching. The polarization measurement results of stretched films fitted well with trigonometric function. Ge *et al.* [119] reported that the aligned CdSe@CdS NRs in polyvinylidene fluoride (PVDF) films show a DOP of 0.52. Then they used the composite film as the downshifting material for polarization-sensitive UV detection. Fig. 11k gives the schematic diagram of the construction of the CdSe@CdS/PVDF composite films. Fig. 11l shows the angle-dependent emissions of the composite films before and after stretching. The DOP increased four and five times for the films stretched to lengths two and

four times that of the original, respectively.

Electrospinning

Electrospinning is a versatile, easy and viable technique to fabricate composite nanofibers, with advantages of both the continuous production and wide application [125–131]. More importantly, the aligned composite nanofibers could be used for polarized light emission.

Jiang *et al.* [132] adopted the electrospinning method to realize *in situ* fabrication of $Cs_3Cu_2I_5$ nanostructures embedded in PVDF films for polarized light emission. The polymer PVDF films can also protect the $Cs_3Cu_2I_5$ nanomaterials. Due to the directional transition dipole moment induced by the anisotropic crystal structure of aligned $Cs_3Cu_2I_5$ nanomaterials and dielectric confinement effect of the PVDF polymer film, the $Cs_3Cu_2I_5$/PVDF composite nanofibers exhibit a high DOP of 0.4. Fig. 12a shows the schematic diagram of the fabrication of $Cs_3Cu_2I_5$/PVDF composite nanofibers by the electrospinning method. Using the polarization measurement setup in Fig. 12b, they demonstrated the maximum DOP of the nanofiber film can reach 0.40, while it is only 0.18 for the microfiber film. Their polarization properties are shown in Fig. 12c, d.

Meng *et al.* [133] reported an *in-situ* fabrication of $MAPbX_3$@polyvinyl alcohol (PVA) nanofibers through electrospinning. The strongly polarized emission of optimized $MAPbX_3$@PVA nanofibers can be attributed to the quantum confinement and dielectric confinement effects. Moreover, a DOP of 0.42 was achieved for the films of well-aligned $MAPbX_3$@PVA nanofibers with a macroscale size. Fig. 12e shows the schematic diagram of the fabrication of $MAPbX_3$@PVA nanofibers by the electrospinning method. From the scanning electron microscopy (SEM) image in Fig. 12f, we can see the $MAPbX_3$@PVA nanofibers are uniform and smooth. The emission anisotropy of the $MAPbX_3$@PVA nanofiber film with different precursor concentrations is shown in Fig. 12g. Fig. 12h–j show the fluorescent optical microscopy images of $MAPbX_3$@PVA nanofiber films, demonstrating that the electrospinning method can be used to fabricate perovskite nanofibers with macroscale alignment. Meng's group [134] fabricated inch-size aligned $MAPbX_3$@PVA nanofiber films by adapting an electrospinning technique. The aligned electrospun polyurethane fibers containing $CsPbBr_3$ NWs also show a high DOP of 0.30 [135]. Hasegawa *et al.* [136] fabricated the nanofiber sheets consisting of aligned electrospun polymer nanofibers embedded with CdSe/CdS NRs. The DOP of the nanofiber sheets can be up to 0.6. Aubert *et al.* [137] embedded silica-coated CdSe/CdS NRs in polymeric nanofibers by electrospinning, and achieved large-scale and electrically switchable polarized emission.

Photoalignment

The photoalignment method can achieve precise alignment of

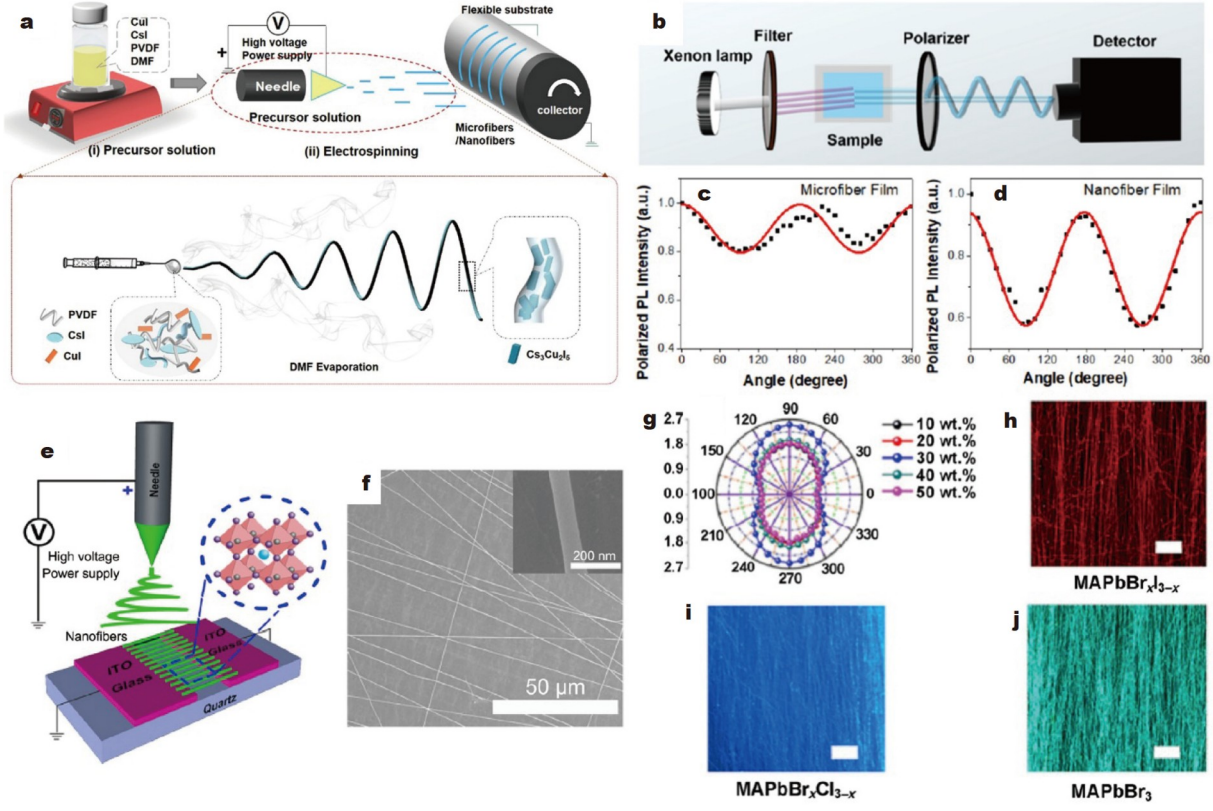

Figure 12 (a) Schematic diagram of the fabrication of $Cs_3Cu_2I_5$/PVDF composite nanofibers by the electrospinning method. (b) Setup for the polarization measurement of composite nanofibers. PL intensities of (c) microfiber and (d) nanofiber films as a function of polarizer angle. Reprinted with permission from Ref. [132], Copyright 2022, American Chemical Society. (e) Schematic diagram of the electrospinning setup for the fabrication of $MAPbX_3$@PVA nanofibers. (f) SEM image of $MAPbBr_3$@PVA nanofibers. (g) Polarized emission of the aligned $MAPbBr_3$@PVA nanofiber films with different precursor concentrations. (h–j) Fluorescent optical microscopy images of $MAPbX_3$@PVA nanofiber films (scale bars are 100 μm). Reprinted with permission from Ref. [133], Copyright 2019, Springer Nature.

nanomaterials in the desired position at the nanoscale, because the photo-reorientation of chromophores offers large anchoring energy with a low pretilt angle [7,138,139]. Besides, the linear arrays of smectic liquid crystal defects can play a role of smart matrix to manipulate the position and direction of NRs [140]. Fig. 13a shows the straightforward but multistep process of the photoalignment of the NRs in the liquid crystal polymer films [7]. This process includes spin coating and subsequent photoalignment, after spin coating a mixture of nanomaterials and liquid crystal polymer monomers in toluene, the polymerization under UV light would ensure the stability of the composite films. The photoinduced surface energy of the alignment layer gives a torque to the liquid crystal polymer molecules and aligns them in the direction parallel to the easy axis of the chromophore. Meanwhile, the repulsive intermolecular forces between the nanomaterial ligands and liquid crystal polymer molecules would exert counter-torque, and align the nanomaterials perpendicular to the easy axis of the chromophore. The polarization angle dependences of the emission intensity for red and green films are presented in Fig. 13b, c, respectively, which show good agreement with the Malus's law.

The photoalignment approach also offers the possibility to align the light emitting nanomaterials on patterned surfaces. Schneider *et al.* [138] used photoalignment to align CdSe/CdS core-shell NRs dispersed in a liquid crystal polymer into microscale patterns. After unidirectional alignment, the patterns were fabricated by a second irradiation with different polarization azimuths and the employment of a photomask. Fig. 13d presents the concept of the angular dependence of the emission intensity for 2D fluorescent grating patterns. Depending on the directions of the NRs and excitation polarization, the patterns exhibit the variation of dark and bright states. When the excitation polarization azimuth is 45°, the absorption and emission intensities are equal. The fluorescence micrographs show the minimum (dark) and maximum (bright) states when the polarization azimuth is 0° and 90°, respectively.

Mechanical rubbing

The mechanical rubbing is a very simple and convenient method to align NRs on large scales [50,141,142]. During rubbing process, the dragging force produced by the rubbing fibers leads to deflection and reorientation of the NRs along the direction of rubbing. However, the relatively rough films constructed by this method are to some extent difficult to achieve high EQE for LEDs.

Amit *et al.* [141] reported the alignment of CdSe/CdS semiconductor NR film for macroscopic scale through this method. Fig. 14a shows the schematic of the mechanical rubbing process. Fig. 14b gives the SEM image of CdSe/CdS semiconductor NR film characterized by the random NR orientation. After mechanical rubbing, the NRs are aligned along the rubbing direction (Fig. 14c). They studied the effects of substrate treatments on the DOP and showed that partially hydrophobic surface is beneficial for the alignment of CdSe/CdS NRs. In

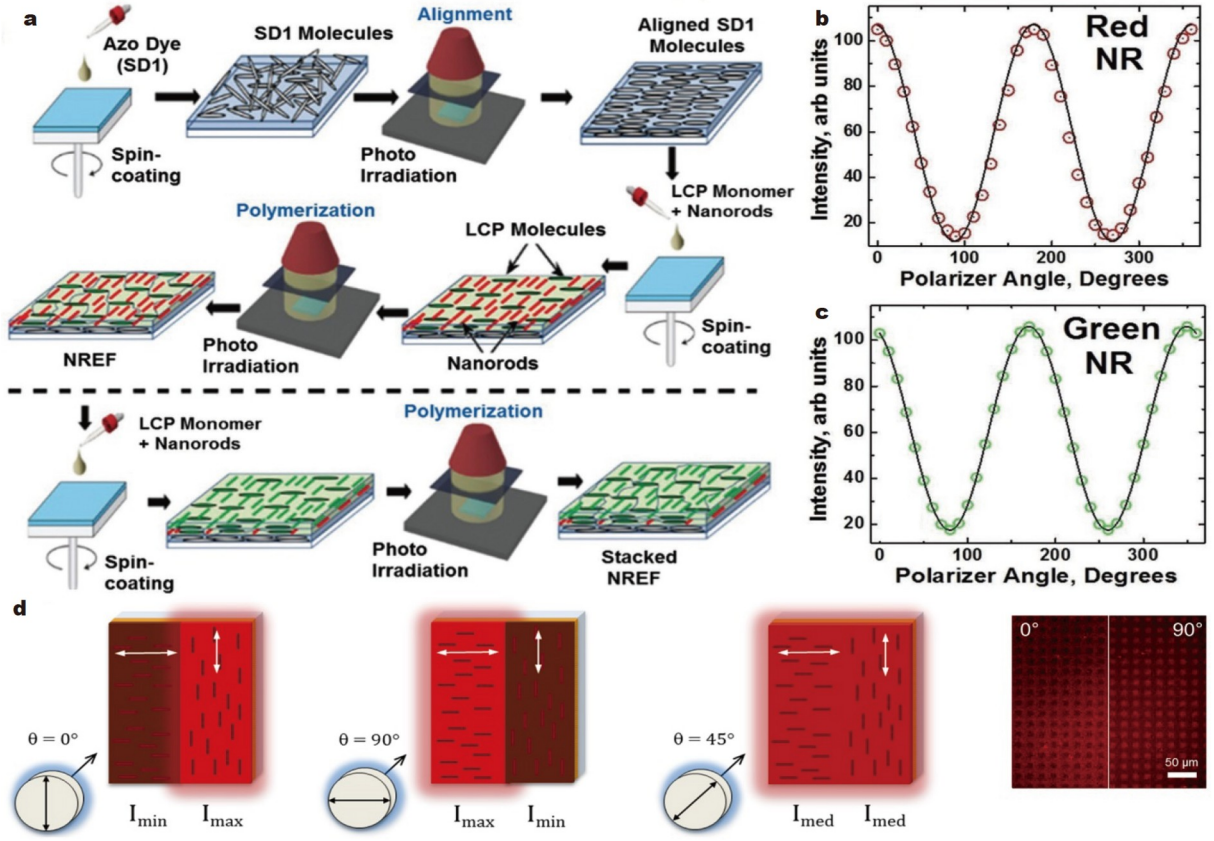

Figure 13 (a) Processing flow of the photoalignment of the NRs in the liquid crystal polymer films. PL intensities of (b) red and (c) green NR films as a function of polarizer angle. Reprinted with permission from Ref. [7], Copyright 2017, Wiley-VCH Verlag GmbH & Co. KGaA, Weinheim. (d) Schematic illustration of the angular dependence of the emission intensity for 2D fluorescent grating patterns. Reprinted with permission from Ref. [138], Copyright 2017, American Chemical Society.

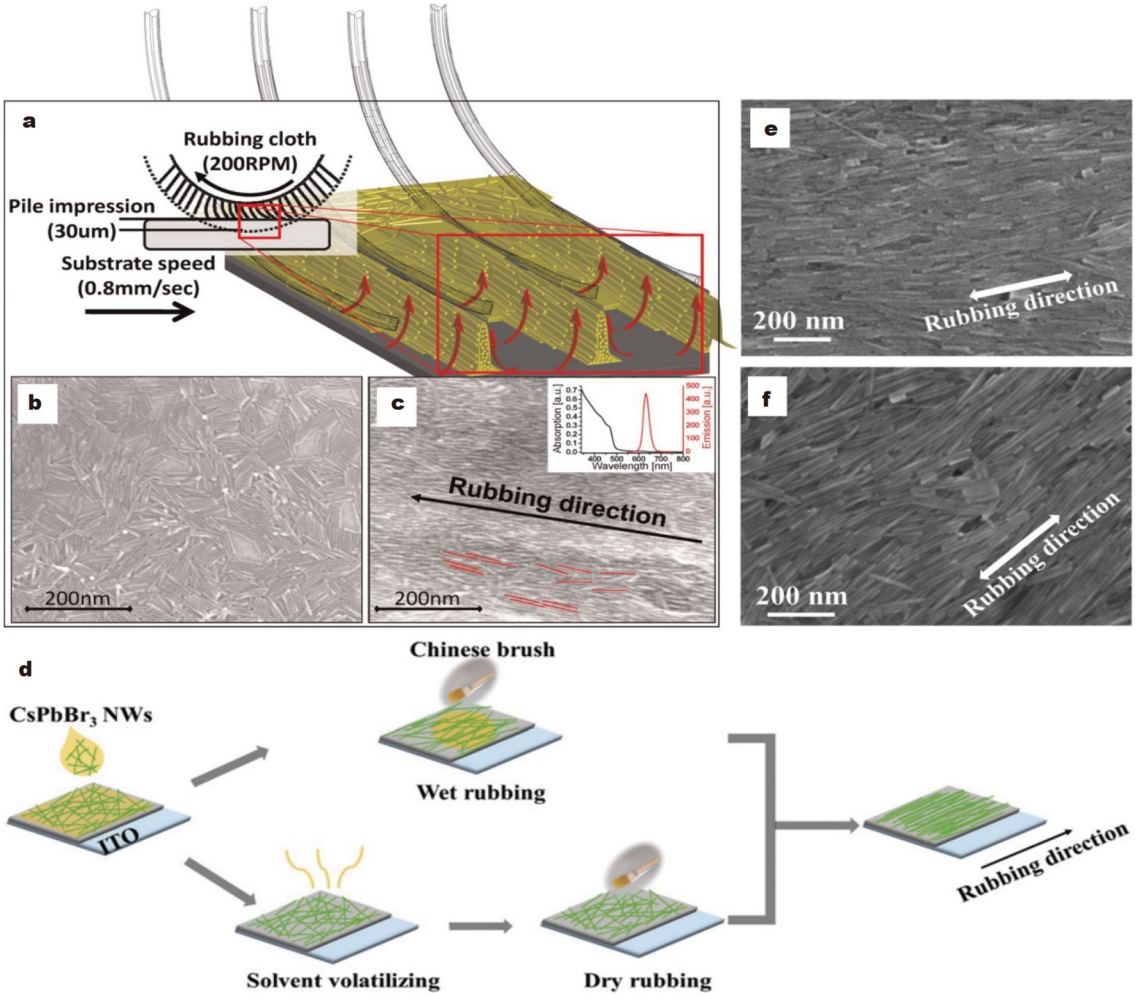

Figure 14 (a) Schematic of the mechanical rubbing process. (b) SEM image of spin-coated CdSe/CdS semiconductor NR film. (c) SEM image of rubbed CdSe/CdS semiconductor NR film. Reprinted with permission from Ref. [141], Copyright 2012, Wiley-VCH Verlag GmbH & Co. KGaA, Weinheim. (d) Schematic diagram of $CsPbBr_3$ NW films prepared by mechanical dry rubbing and wet rubbing. SEM images of $CsPbBr_3$ NW films after mechanical (e) wet rubbing and (f) dry rubbing. Reprinted with permission from Ref. [50], Copyright 2020, The Royal Society of Chemistry.

addition, the optimal amount of organic ligands added to the deposited solution was found to yield high-quality alignment. The prepared CdSe/CdS film exhibited high linearly polarized emission with a DOP of 0.56. While the contrast experiments of rubbed spherical QDs and spin-coated films of NRs exhibited no polarized light emission. Wei *et al.* [50] aligned $CsPbBr_3$ anisotropic NWs using the mechanical rubbing method. Fig. 14d shows the schematic diagram of the preparation process for aligned $CsPbBr_3$ films by mechanical dry rubbing and mechanical wet rubbing methods. Fig. 14e, f show the SEM images of $CsPbBr_3$ NW films after mechanical wet rubbing and mechanical dry rubbing, respectively. The directions of NWs are in accordance with the rubbing directions for both wet rubbing and dry rubbing methods. The dry-rubbed film shows a little lower polarization PL behavior with a DOP of 0.50. At last, they also used the dry-rubbed film for polarized LED device fabrication.

Self-assembly at the liquid/air interface

Usually, the surface tension of liquid is used in this method to achieve self-assembly. Rizzo *et al.* [49] developed a simple and effective method to assemble colloidal CdSe/CdS NRs on the surface of water (Fig. 15a). This technique includes two steps. Firstly, the CdSe/CdS NR solution is floated onto a water surface. During the solvent evaporation process, the NRs in the concentrated organic solution would self-assemble into an ordered NR film at the liquid/air interface. Secondly, a polydimethylsiloxane (PDMS) stamp is used to fish and transfer the NR film by contact printing from the water surface. By exploiting this contact printing method, they fabricated an LED with strongly polarized emission. Kim *et al.* [143] developed a simple method to make optically anisotropic films by shear-oriented assembly of $LaPO_4$ NRs. Fig. 15b illustrates a schematic of the customized coating machine. In this method, shearing a thixotropic rod gel may induce such a gel-to-sol transition and simultaneously the orientation of rods as they recover the individual mobility. Firstly, a certain amount of NR solution was dropped onto the substrate. Secondly, the substrate was dragged under the coating blade at a constant speed and a fixed distance from the blade plane. The film thickness can be well controlled by the gap thickness. Then, the substrate with sheared suspension was heated to 140°C to evaporate the solvent. At last, the solidified film was annealed at 500°C for 2 h. Deng *et al.* [144] aligned perovskite NWs by a modified evaporation-induced self-

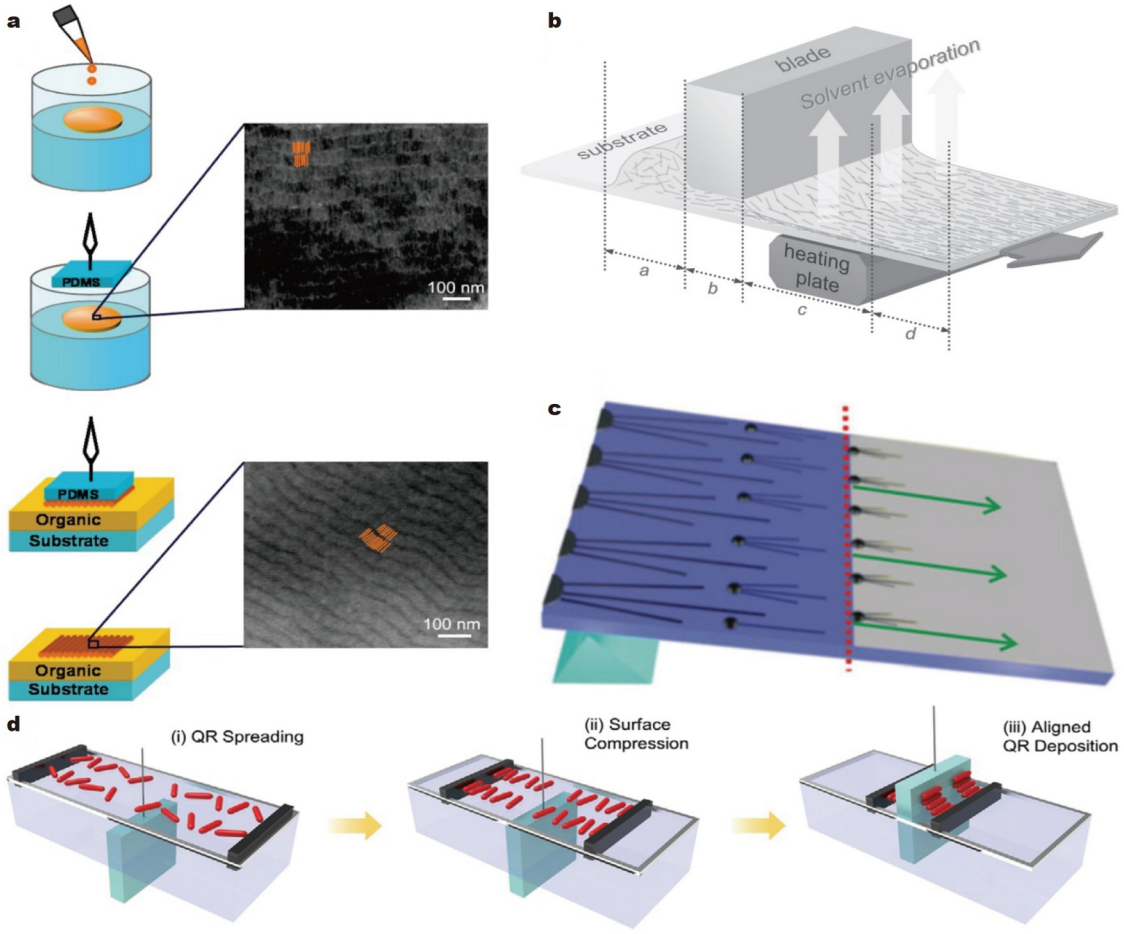

Figure 15 (a) Schematic diagram of the method for the deposition of aligned NR arrays on organic layers. Reprinted with permission from Ref. [49], Copyright 2009, American Chemical Society. (b) Schematic diagram of the fabrication of aligned NR thin films by the blade-coating process. Reprinted with permission from Ref. [143], Copyright 2013, Wiley-VCH Verlag GmbH & Co. KGaA, Weinheim. (c) Schematic diagram of the aligned NW growth by evaporation-induced self-assembly. Reprinted with permission from Ref. [144], Copyright 2015, The Royal Society of Chemistry. (d) Schematic diagram of the aligned NR film by the Langmuir-Blodgett technique. Reprinted with permission from Ref. [48], Copyright 2021, Wiley-VCH Verlag GmbH & Co. KGaA, Weinheim.

assembly method. The growth mechanism is schematically described in Fig. 15c. The possible growth mechanisms are as follows. At the beginning, the NWs grow from the edge of the substrate due to the heterogeneous nucleation growth. As evaporation continues, the liquid/substrate interface line driven by evaporation and gravity moves along the evaporation direction. As a result, the NWs can be aligned very well quasi-vertically to the substrate edge.

Langmuir-Blodgett assembly is a simple and feasible method to assemble monolayer films in a large-area at the water/air interface [145]. The constructed films can be transferred to various substrates. Rhee *et al.* [48] carefully optimized the Langmuir-Blodgett technique deposition condition and achieved highly dense and smooth NR thin film. Fig. 15d shows the deposition process of NR film by the Langmuir-Blodgett method. Firstly, amphiphilic NRs dissolved in hexane were dropped in the Langmuir-Blodgett trough filled with deionized water. The NRs will rapidly spread on the water surface without sinking or mixing. Secondly, after evaporation of the hexane, the two barriers were moved toward the center so as to compress the floating NR film. The increased surface pressure is helpful to form highly dense film on the surface of water. Thirdly, a pre-immersed substrate was pulled up slowly to transfer the aligned NR film to the substrate. The DOP of thin film with high order of alignment of NRs is 0.21.

However, because water is used during the preparation process, this method cannot be used to assemble perovskite nanomaterials directly because of their poor stability. The chemical surface modification by a protection layer with strong affinity should be a reasonable method not only to obtain individually dispersed NWs with good water stability but also to retain the optoelectronic properties of NWs. Liu *et al.* [145] introduced an amphiphilic block copolymer to modify the surface of $CsPbBr_3$ NWs. The surface-modified core shell perovskite NWs revealed enhanced photoluminescent emission and stability against water. Afterwards, they further applied the Langmuir-Blodgett method to assemble highly aligned NW monolayer. At last, they achieved a DOP of 0.36 in the aligned monolayer.

Electric field-assisted assembly

Electric field-assisted assembly can align anisotropic nanomaterials with high uniformity under the action of local electric fields [86,146–150]. However, the disadvantages for this method could be the smaller size of the film and the requirement of

patterned substrate [146–148]. Hu *et al.* [146] reported a method to control the position and orientation of colloidal CdTe and CdSe NRs by the local electric fields generated from an interdigitated electrode. Fig. 16a shows the schematic of the device. Different electric fields could be achieved by varying the width (W) and length (L) of the device. Fig. 16b shows the schematic of the experiment. A drop of hexane/octane solution containing NRs dries on the surface while voltage is applied to the electrodes. They reveal strong alignment of NRs to the direction of the applied field and dense accumulation around and onto the voltage-biased electrodes (Fig. 16c). The degree of alignment under the applied electric field is quantified by a nematic order parameter $S \approx 0.8$ in contrast to the zero-field case where $S \approx 0.1$. Carbone *et al.* [86] also assembled their synthesized CdSe/CdS dot-in-rod core-shell NRs in the lateral and vertical directions on the substrates up to micrometer-size. Fig. 16d, e show the lateral alignment of NRs with electric fields. The red arrow represents the direction of the applied electric field. At last, a DOP of 0.45 is observed on micrometer scale.

Kaur *et al.* [147] fabricated a functional film on the interdigitated electrode substrate to align CdSe/CdS NRs. Fig. 16f illustrates the steps for the formation of the NR film. Without the applied electric field, the reactive mesogen molecules are randomly oriented. As the voltage increases, the reactive mesogen molecules are driven by the external bias to minimize the electrostatic energy of the system. The applied electric field can control the position and orientation of NRs. Then, the NRs are fixed in position by the polymerization under the exposure of UV light. The DOP of aligned NRs was measured to be 0.48. Persano *et al.* [148] fabricated aligned CdSe/CdS core/shell NR film by drop casting the NRs from a solution on substrates with prepatterned electrodes. Fig. 16g, h show the SEM images of aligned CdSe/CdS NRs at different magnifications. Gryn *et al.* [149] showed anisotropic NRs can be aligned and organized in a large area by anisotropic interactions with the bulk molecular director and linear topological defects. Mohammadimasoudi *et al.* [150] produced a hybrid luminescent layer based on CdSe/CdS NRs dispersed in a liquid crystal. Then, the NRs are aligned by applied electric field and polymerized by UV illumination. The DOP of the CdSe/CdS NR film can be up to 0.6.

Template-assisted assembly

The template-assisted assembly method can be used to fabricate polarized light emitting films, but it is not compatible with the standard LED fabrication process. Wang *et al.* [151] aligned a needle-like superparticle structure into unidirectional line patterns on Si_3N_4 substrates through capillary forces (Fig. 17a, b). Furthermore, the patterns can be readily transferred into uniform and removable thin films of PDMS with large size. The resulting thin films exhibit strong polarized light emission with a high DOP of 0.88, which is much higher than that of individual single CdSe/CdS NRs (Fig. 17c). This enhanced polarized light emission mechanism can be attributed to the combination of the dielectric effect and collective electric dipole coupling effects among the CdSe/CdS NRs inside the elongated needle-like superparticle structure embedded in PDMS films.

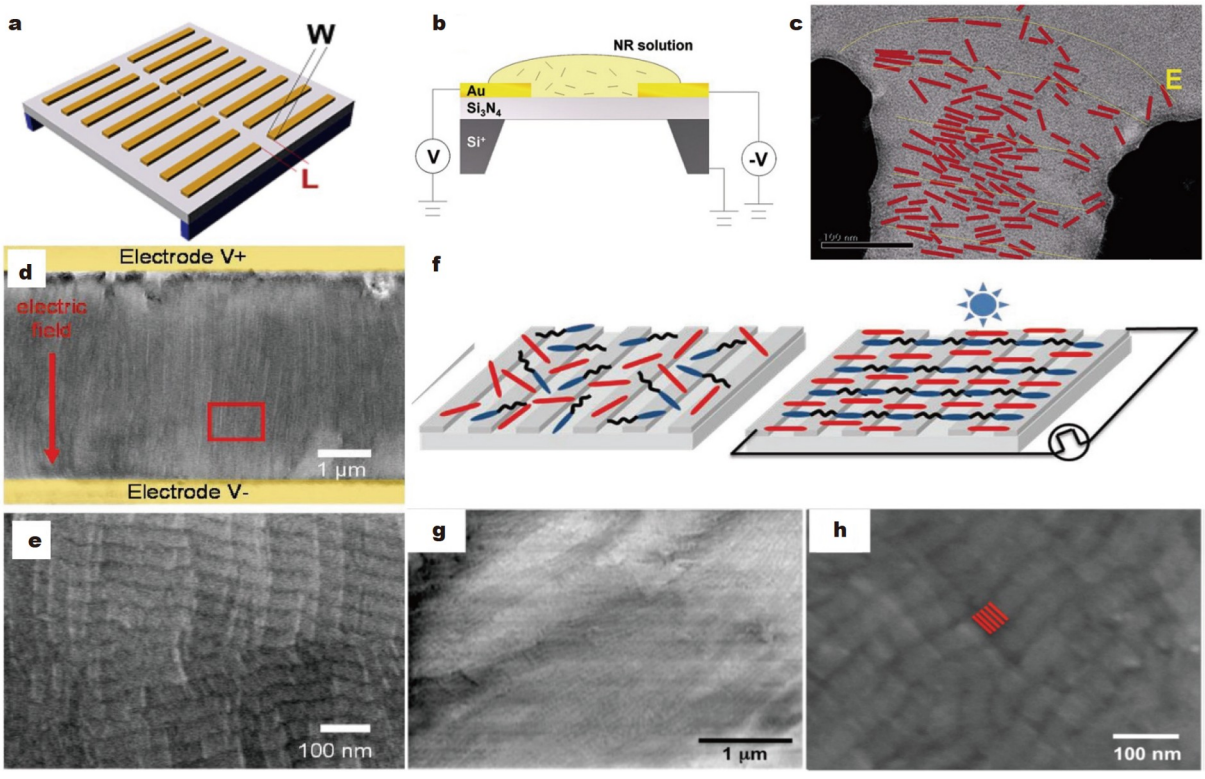

Figure 16 (a) Schematic of a device containing eight patterned electrode pairs with different gap widths and lengths. (b) Schematic of the experiment. (c) TEM image of the electric field-driven alignment of NRs. Reprinted with permission from Ref. [146], Copyright 2006, American Chemical Society. (d, e) SEM images of aligned CdSe/CdS NRs at different magnifications. The red arrow indicates the direction of electric field. Reprinted with permission from Ref. [86], Copyright 2007, American Chemical Society 2007. (f) Steps for the formation of NR film by the electric-field-aided aligned assembly method. Reprinted with permission from Ref. [147], Copyright 2018, Wiley-VCH Verlag GmbH & Co. KGaA, Weinheim. (g, h) SEM images of oriented CdSe/CdS NRs at different magnifications. Reprinted with permission from Ref. [148], Copyright 2010, American Chemical Society.

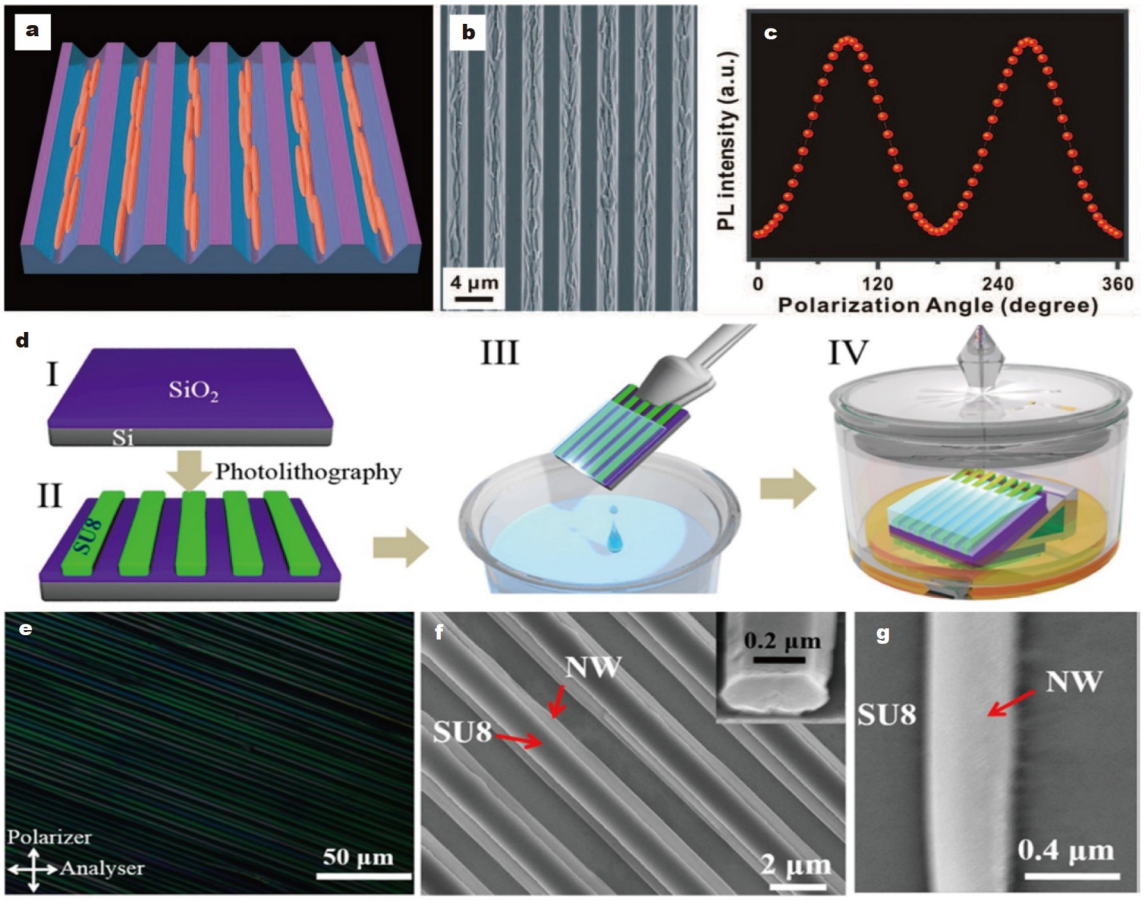

Figure 17 (a) Schematic diagram for aligning the superparticles into the unidirectional line patterns. (b) SEM image of the superparticles inside a line pattern. (c) PL intensity of superparticle film as a function of polarizer angle. Reprinted with permission from Ref. [151], Copyright 2012, American Association for the Advancement of Science. (d) Schematic diagram of the fabrication $MAPbI_3$ NW array by a facile fluid-guided antisolvent vapor-assisted crystallization method. (e) Cross-polarized optical micrograph of $MAPbI_3$ NW array. (f) SEM image of the $MAPbI_3$ NW array grown on two sides of photoresist strips. (g) Magnified SEM image of the NW. Reprinted with permission from Ref. [152], Copyright 2017, American Chemical Society.

The template-assisted assembly method can also be used to produce highly aligned single-crystalline $MAPb(I_{1-x}Br_x)_3$ (x = 0, 0.1, 0.2, 0.3, 0.4) NW arrays with a continuously adjustable absorption range from 680 to 780 nm [152]. Deng *et al.* [152] used the periodically aligned SU-8 photoresist stripes on the SiO_2/Si substrate as the template to fabricate the $MAPb(I_{1-x}Br_x)_3$ perovskite NWs by a facile fluid-guided antisolvent vapor-assisted crystallization method. The schematic illustration of the preparation method is shown in Fig. 17d. The SU-8 template is dipped into $MAPbI_3$/DMF solution and then placed in the CH_2Cl_2 solvent. The diffusion of antisolvent leads to the precipitation of $MAPbI_3$ NCs along the sides of SU-8 template. Fig. 17e shows the large-area continuous and uniform NW arrays. From the SEM image in Fig. 17f, we can see the aligned $MAPbI_3$ NWs are preferentially deposited on the two sides of SU-8 template rather than the channels. The magnified SEM image shows that the $MAPbI_3$ NW has smooth surface (Fig. 17g). Lutich *et al.* [153] fabricated highly ordered CdSe/CdS core-shell NRs by infiltration of the NRs into the pores of transparent porous anodic alumina membrane. The CdSe/CdS NR films have highly polarized PL and absorption properties.

Off-center spin-coating

Off-center spin-coating is a very simple strategy to align anisotropic nanomaterials. It has large potential in the polarized LED, because it is compatible with the standard LED fabrication process. Yuan *et al.* [154] developed the method of off-center spin-coating. As shown in Fig. 18a, in this method, the substrate is placed far away from the center of the spin coater. When the spin coater begins to rotate, the nanomaterials in the solution could be aligned by the outward centrifugal force. Spin-coating is widely used in the LED fabrication due to its easy process, high quality film and free of the complicated film transfer process. Off-center spin-coating combines the advantages of spin-coating and oriented assembly. Even though there is only one study using this method to fabricate LED so far, we believe it is a very promising approach [155]. Kim *et al.* [156] prepared highly aligned organic polymer semiconductor films by off-center spin-coating of the pre-aggregated conjugated polymer solution. Fig. 18b shows the schematic illustration of aligned polymer films under the action of centrifugal force. Fig. 18c shows the SEM image of the aligned $CsPbBr_3$ NW films prepared by off-center spin-coating [155]. However, the quality of $CsPbBr_3$ NW film is still far from satisfactory. Because the organic ligand on the surface of NWs would cause strong van der Waals force between adjacent NWs. At last, the resulted $CsPbBr_3$ NW bundles will inevitably reduce the film quality. Furthermore, this method can also be used to align silver, silicon NWs and poly-

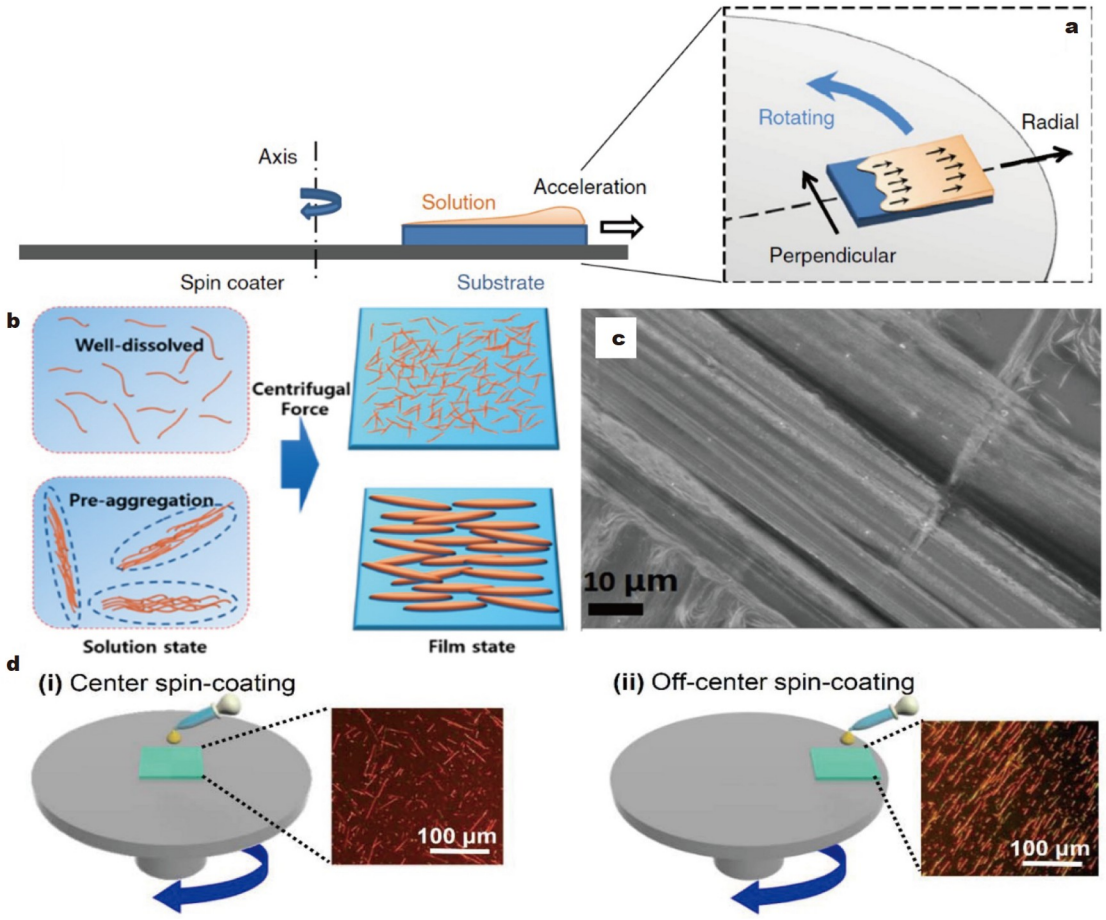

Figure 18 (a) Schematic diagram of the off-center spin-coating method. Reprinted with permission from Ref. [154], Copyright 2014, Nature Publishing Group. (b) Schematic diagram of aligned polymer films under the action of centrifugal force. Reprinted with permission from Ref. [156], Copyright 2015, American Chemical Society. (c) SEM image of the $CsPbBr_3$ NW film prepared by off-center spin-coating. Reprinted with permission from Ref. [155], Copyright 2020, Elsevier B.V. (d) Schematic diagrams of conventional spin-coating, off-center spin-coating and polarized optical microscopy images of Si NWs. Reprinted with permission from Ref. [158], Copyright 2022, MDPI.

mer chains [157–159]. Fig. 18d compares the silicon NW alignment effects made by the conventional spin-coating and off-center spin-coating methods. From the optical microscopy images, we can see the ordered silicon NWs outward the radial direction made by off-center spin-coating.

POLARIZED LIGHT EMISSION LEDs

The practical use of polarized light emission LEDs in the display industry can eliminate the need of a front polarizing film, which reduces the manufacturing cost and time. As mentioned earlier, many methods have been used to achieve polarized light emission in aligned anisotropic nanomaterials, but some of the aligning methods are not compatible with the standard LED fabrication process, leading to poor device performance. Therefore, it is urgently needed to identify effective methods to align anisotropic nanomaterials without destroying the LED structure, thereby achieving high-performing polarized LEDs. In this section, we would summarize and compare several different methods to construct polarized light emission LEDs in two parts: the II–VI colloidal nanomaterials-based polarized LEDs and the perovskite nanomaterials-based polarized LEDs.

II–VI colloidal nanomaterials-based polarized LEDs

Hikmet *et al.* [40] constructed the first polarized light emission LED in 2005. They used the core/shell CdSe/CdS NRs with a PLQY about 50% as the emitting layer. The CdSe/CdS NRs are aligned by rubbing. Fig. 19a shows the electroluminescence (EL) spectrum of the polarized LED in the parallel and perpendicular directions to the rubbing. Obviously, the parallel direction has stronger emission intensity. However, the blue emission from polyvinylcarbazole (PVK) can also be seen in the spectrum, indicating some electron-hole pair recombination around the PVK interface. Rizzo *et al.* [49] also constructed a polarized LED based on highly ordered arrays of colloidal CdSe/CdS core/shell NRs as the active species. The alignment method for CdSe/CdS film is discussed before. Then this technique was used to transfer floating NR film onto an organic layer to fabricate polarized LED. The inset of Fig. 19b shows the device structure. Fig. 19b shows the current voltage and luminance voltage properties of NR LED. The maximum brightness of 170 cd m^{-2} achieves at 19 V and 140 mA cm^{-2}. The EL spectrum reveals that the light emission comes from the CdSe/CdS NRs. The inset of Fig. 19c compares the EL spectra for parallel and perpendicular directions.

Rhee *et al.* [48] reported polarized EL emission based on high-performance CdSe/CdS NR LED. The Langmuir-Blodgett technique they used to obtain highly dense and smooth NRs thin film is discussed in section "Self-assembly at the liquid/air

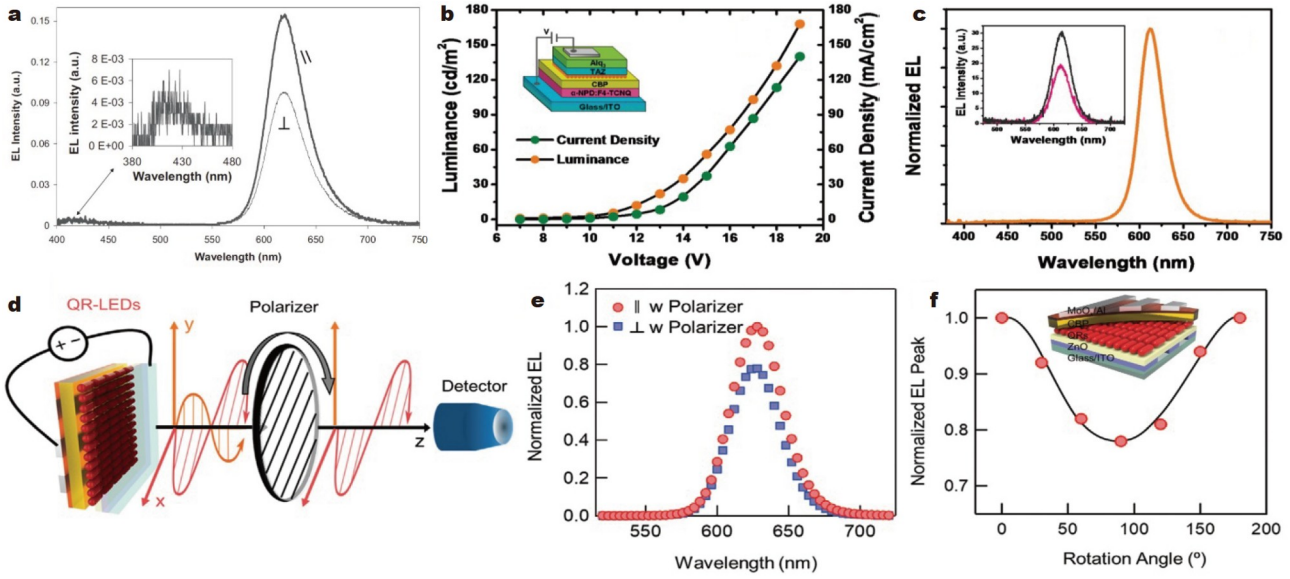

Figure 19 (a) EL spectra of the polarized LED in the parallel and perpendicular to the rubbing direction. Reprinted with permission from Ref. [40], Copyright 2005, Wiley-VCH Verlag GmbH & Co. KGaA, Weinheim. (b) Current voltage and luminance voltage properties of the aligned NR LED. The inset shows the device structure. (c) EL spectrum. The inset shows the EL spectra for parallel and perpendicular directions. Reprinted with permission from Ref. [49], Copyright 2009, American Chemical Society. (d) Experimental setup for measuring polarized LED under electrical excitation. (e) EL spectra of the LED fabricated by the Langmuir-Blodgett technique in the parallel and perpendicular to the alignment directions of NRs. (f) EL peak intensity of the LED as a function of rotational angle. Reprinted with permission from Ref. [48], Copyright 2021, Wiley-VCH Verlag GmbH & Co. KGaA, Weinheim.

interface" in detail. Fig. 19d shows the experimental setup for measuring polarized LED under electrical excitation. A linear polarizer is placed between the LED device and detector, and the EL intensities of different angles can be measured by rotating the polarizer from 0° to 180°. A constant current should be applied to maintain the EL of LED during the measuring process. As can be seen in Fig. 19e, the EL spectrum exhibits 1.25-fold higher intensity when the polarizer is parallel to the alignment direction of NRs. Fig. 19f shows the peak intensity with respect to the rotational angle. At last, the polarized LED fabricated by the Langmuir-Blodgett technique shows a low turn-on voltage of 1.85 V, a decent peak EQE of 10.33%, and a high maximum luminance of 56,287 cd m^{-2}. This is the highest EQE of polarized LED ever reported. Compared with spin coating, this method just causes a slight deterioration of the device performance. It can be attributed to the degradation of CdSe/CdS NRs during the assembly process in water surface. Therefore, this method is not applicable to perovskite materials.

Perovskite nanostructure-based polarized LEDs

Due to their excellent photoelectric properties and promising applications, anisotropic perovskite nanomaterials have also drawn significant attention in polarized LEDs. However, some methods of constructing polarized light emitting films discussed above are inapplicable to perovskite nanomaterials because of their instability. The mechanical rubbing and off-center spin-coating are the only two methods used to fabricate $CsPbBr_3$ NWs polarized LED for now. Nevertheless, because of the strict requirements on the film quality of LED devices, the perovskite nanostructure-based polarized LEDs prepared by these two methods have not achieved desired results. Wei *et al.* [50] successfully fabricated $CsPbBr_3$ NWs polarized LED using a mechanical rubbing method in 2020. Fig. 20a, b show the luminance-voltage and current density-voltage characteristics of the $CsPbBr_3$ NW LEDs. The inset of Fig. 20a shows the device structure of polarized LED. Combined with an optimal device structure, the turn-on voltage has been as low as 6.5 V. They studied the device performances with different hole transport materials and found the single-layer poly-TPD-based device showed the best device performance. However, the highest EQE was only 0.08%. Then, they used the off-center spin-coating method to align $CsPbBr_3$ NW films and fabricated the polarized LED [155]. Fig. 20c shows the EL spectrum dependence of the voltage. The emission peak is located at 523 nm. The film quality and device performance in this work need to be further enhanced.

CURRENT CHALLENGES IN THE POLARIZED LIGHT EMISSION LEDs

Effective aligning methods compatible with the standard LED fabrication process

Table 1 summarizes the polarized LEDs' performance based on different materials and assembly methods. As can be seen, the fabricated polarized light emission LEDs still have some problems until now: the low efficiency and DOP, which are most significantly affected by the aligning method of anisotropic nanomaterials. In this review, we have discussed many methods of aligning anisotropic nanomaterials to construct polarized light emitting films. However, some of the aligning methods produce limited anisotropic nanomaterials alignment, irregular and low-quality films, introduction of other assisting materials and, most importantly, are not compatible with the standard LED fabrication process, leading to poor device performance. Overall, we put great expectation on off-center spin-coating and electric field-assisted assembly to align anisotropic nanomaterials without destroying the LED structure, thereby achieving high-efficiency polarized LEDs.

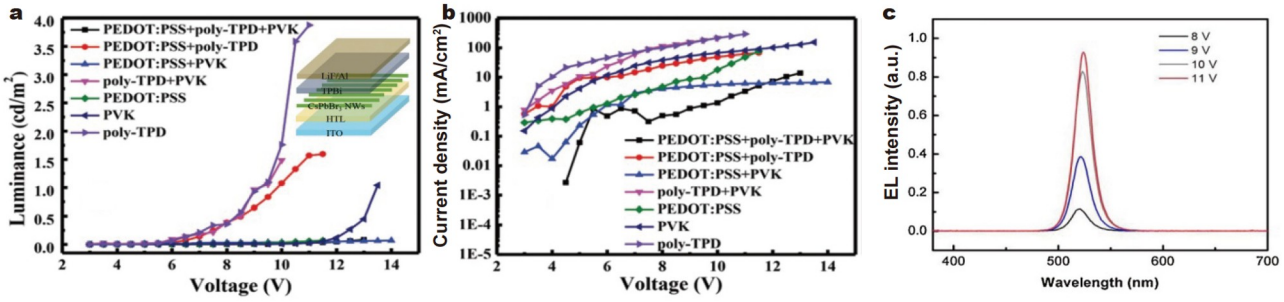

Figure 20 (a) Luminance-voltage and (b) current density-voltage characteristics of the $CsPbBr_3$ NW LEDs. The inset of (a) shows the device structure of polarized LED. Reprinted with permission from Ref. [50], Copyright 2020, The Royal Society of Chemistry. (c) EL spectra of the $CsPbBr_3$ NW LED under different voltage biases. Reprinted with permission from Ref. [155], Copyright 2020, Elsevier B.V.

Table 1 Summarized polarized LEDs performance based on different materials and assembly methods

Year	Material	Assembly method	Device structure	DOP of film	DOP of device	EQE	Ref.
2005	CdSe/CdS	Rubbing	ITO[a]/PEDOT[b]/PVK/NRs/TPBI[c]/Ba/Al	0.38	0.23	0.49%	[40]
2009	CdSe/CdS	Self-assembly	ITO/α-NPD:F4-TCNQ[d]/CBP[e]/NRs/TAZ[f]/Alq_3[g]/LiF/Al	0.34	~0.2	–	[49]
2020	$CsPbBr_3$	Off-center spin-coating	ITO/PEDOT/poly-TPD[h]/NWs/TPBI/LiF/Al	0.46	–	–	[155]
2020	$CsPbBr_3$	Mechanical rubbing	ITO/PEDOT/poly-TPD/PVK/NWs/TPBI/LiF/Al	0.50	–	0.08%	[50]
2021	CdSe/CdS	Langmuir-Blodgett	ITO/ZnO/NRs/CBP/MoO_x/Al	0.26	0.11	10.33%	[48]

a) ITO: indium tin oxide; b) PEDOT: poly(3,4-ethylenedioxythiophene); c) TPBI: 2′,2′-(1,3,5-benzinetriyl)-tris(1-phenyl-1-*H*-benzimidazole); d) α-NPD:F4-TCNQ, *N*,*N*′-bis(naphthalen-1-yl)-*N*,*N*′-bis(phenyl)benzidine:2,3,5,6-tetrafluoro-7,7,8,8-tetracyano-quinodimethane; e) CPB: 4,4′,*N*,*N*′-diphenylcarbazole; f) TAZ: 3-(4-biphenylyl)-4-phenyl-5-*t*-butylphenyl-1,2,4-triazole; g) Alq_3: tris(8-(hydroxyl-quinoline) aluminum; h) poly-TPD: poly[bis(4-phenyl)(4-butylphenyl)amine].

Spin-coating is a mature method and widely used in the LED fabrication. Off-center spin-coating has a large potential in the polarized LED, because it combines the advantages of easy process, high-quality film and free of complicated film transfer process from spin-coating and oriented assembly from other methods. The only one study using this method did not achieve high LED performance, because the surface organic ligand of NWs would cause the $CsPbBr_3$ NWs to form big bundles, so as to reduce the film quality, whereas a proper surface ligand treatment may solve this problem and then induce uniform films.

Electric field-assisted assembly has been proved to align anisotropic nanomaterials with high uniformity under the action of local electric fields. The problems for this method could be the smaller size and patterned substrate. The strategy of electric field-assisted assembly combined with dip-coating should be a feasible method. Firstly, the anisotropic nanomaterials can be aligned orderly in solution under applied electric fields. Then, the pre-immersed substrate is pulled up slowly. After drying, the well-ordered NR film can be achieved on the substrate. It should be noted that a slight deterioration of LED performance might occur due to the degradation of transport layer during immersing in NR solution. Highly tolerant transport layers deposited by atomic layer deposition and magnetron sputtering are expected to avoid this damage.

Polarized light emission and charge carrier transport mechanisms for polarized LEDs

The direct cause of polarized light emission for anisotropic nanomaterials is that their radiative transition dipole moments tend to be distributed along their long axis. For PL, the polarized luminescence properties of anisotropic nanomaterials are determined by the quantum confinement effect and dielectric confinement effect, which are related to their lateral size and the dielectric constant of the external environment. With regard to EL, the electron distribution of the anisotropic nanomaterial surface and the environmental permittivity will affect the DOP [160]. Because the anisotropic nanomaterials are perpendicular to the direction of the applied electric field, the applied electric field will inevitably affect the electron distribution and permittivity [161]. The characteristics of the carrier migration in the anisotropic nanomaterials under the action of the electric field force need to be further studied. Therefore, it is vitally important to reveal the mechanisms of polarized light emission and charge carrier transport for polarized LEDs, so as to construct the LEDs with high DOP and EQE [160–164].

Key challenges for the commercial development

Although the self-emissive polarized LEDs have huge market development potentials to meet the demand of future display, the research on polarized LED devices is still in its infancy, and some key challenges for the commercial development still remain in this field. Firstly, high EQEs are necessary for commercial applications of polarized LEDs (especially blue polarized LED). There is still a need to further improve the efficiency by optimizing the device structure, designing suitable transport layer materials, preparing highly ordered light-emitting layers and so on. Secondly, the long-term stability of both nanomaterials and devices for LEDs is a well-recognized challenge, hindering their practical application severely. As we all know,

the perovskites are sensitive to water and oxygen, which will degrade rapidly when exposed to the air. The long-term stability of nanomaterials needs to be further improved by ion doping, surface coating, polymer encapsulation and so on. With regard to polarized LED devices, introducing ion-blocking interlayers and all-inorganic charge transport layers is a feasible strategy to improve the device stability and performance. However, since the source of the instability of polarized LED devices is mainly material-related issues, the development of luminescent materials with good stability is the top priority to ensure high stability of polarized LEDs. Thirdly, methods that enable large-scale production are very popular and necessary for factories, such as spin-coating and spray coating. Besides, the development of nontoxic or low-toxic polarized light emitting materials is also an important challenge.

CONCLUSIONS AND OUTLOOKS

Different from the backlight-based display technology in LCDs, the energy-saving self-emissive polarized LEDs without using polarizers have huge development and display market potentials, which can also meet the demand of future display for high color purity, high resolution, wide color gamut, and so on. Various approaches have been carried out to align anisotropic nanomaterials into films, while the DOP and EQE of polarized LEDs are still limited. The high-quality anisotropic nanomaterial films and effective aligning methods compatible with standard LED fabrication processes are required to fabricate polarized LED with high DOP and EQE. Overall, we have great hopes for methods of modified off-center spin-coating and electric field-assisted assembly mentioned in this review to achieve high-efficiency polarized LEDs.

In this review, we give a comprehensive summary on the state-of-the-art progress in the field of polarized light emission from materials to films and then to LEDs. We start with the brief introduction on the theories of polarized light emission and analyze the factors that influence the DOP. After that, the polarized light emission properties from representative materials of QDs, NRs, NWs and NSs are described. Then, the alignment strategies for constructing polarized light emitting films and LEDs are summarized. Finally, we discuss the current challenges such as effective aligning methods compatible with the standard LED fabrication process, polarized light emission and charge carrier transport mechanisms for polarized LEDs. In summary, we strongly believe the future of polarized LEDs is bright and board, which can bring huge economic benefits. We hope this review will provide a valuable summary for current status of this research direction and stimulate some new insightful ideas for future development of this promising field.

Received 18 September 2022; accepted 3 November 2022; published online 3 February 2023

1 Srivastava AK, Zhang W, Schneider J, *et al.* Luminescent down-conversion semiconductor quantum dots and aligned quantum rods for liquid crystal displays. Adv Sci, 2019, 6: 1901345
2 Vaishnavi M, Vineet K. Display Market By Application (Smartphone & Tablet, Smart Wearable, Television & Digital Signage, PC & Laptop, Vehicle Display, and Others), Technology (OLED, Quantum Dot, LED, LCD, E-PAPER, and Others), Industry Vertical (Healthcare, Consumer Electronics, BFSI, Retail, Military & Defense, Automotive, and Others), Display Type (Flat Panel Display, Flexible Panel Display, and Transparent Panel Display): Global Opportunity Analysis and Industry Forecast, 2021-2031. https://www.alliedmarketresearch.com/display-market
3 Chung CS, Jang SL. Weak-field low-temperature currents calculated by one-particle self-consistent calculation. Int J Nanotechnol, 2014, 11: 4
4 Pickett NL, Gresty NC. Innovation in heavy metal-free quantum dot technology. SID Int Symp Digest Tech Papers, 2017, 48: 562–564
5 Ko YH, Jalalah M, Lee SJ, *et al.* Super ultra-high resolution liquid-crystal-display using perovskite quantum-dot functional color-filters. Sci Rep, 2018, 8: 12881
6 Wang Y, Shi J, Chen J, *et al.* Recent progress in luminescent liquid crystal materials: Design, properties and application for linearly polarised emission. J Mater Chem C, 2015, 3: 7993–8005
7 Srivastava AK, Zhang W, Schneider J, *et al.* Photoaligned nanorod enhancement films with polarized emission for liquid-crystal-display applications. Adv Mater, 2017, 29: 1701091
8 Yang G, Zhong H. Multi-dimensional quantum nanostructures with polarization properties for display applications. Isr J Chem, 2019, 59: 639–648
9 Cunningham PD, Souza Jr. JB, Fedin I, *et al.* Assessment of anisotropic semiconductor nanorod and nanoplatelet heterostructures with polarized emission for liquid crystal display technology. ACS Nano, 2016, 10: 5769–5781
10 Srivastava AK, Zhang W, Schneider J, *et al.* Photo-aligned quantum rod dispersed liquid crystal polymer films. SID Int Symp Digest Tech Papers, 2016, 47: 602–604
11 Wang X, Wang Y, Gao W, *et al.* Polarization-sensitive halide perovskites for polarized luminescence and detection: Recent advances and perspectives. Adv Mater, 2021, 33: 2003615
12 Elkhov VA, Ovechkis YN. Light loss reduction of LCD polarized stereoscopic projection. In: Proc. SPIE 5006, Stereoscopic Displays and Virtual Reality Systems X, Santa Clara, CA, 2003, 45–48
13 Ge Y, Meng L, Bai Z, *et al.* Linearly polarized photoluminescence from anisotropic perovskite nanostructures: Emerging materials for display technology. J Inf Display, 2019, 20: 181–192
14 Luo Z, Xu S, Chen Y, *et al.* Prospects of quantum-dots-based liquid-crystal displays (Invited Paper). Front Matter: Volume 9005. In: Proceeding of SPIE, San Francisco, California, 2014
15 Chen H, Zhu R, Tan G, *et al.* Enlarging the color gamut of liquid crystal displays with a functional reflective polarizer. Opt Express, 2017, 25: 102–111
16 Coe-Sullivan S, Liu W, Allen P, *et al.* Quantum dots for LED down-conversion in display applications. ECS J Solid State Sci Technol, 2012, 2: R3026–R3030
17 Bourzac K. Quantum dots go on display. Nature, 2013, 493: 283
18 Chen N, Bai Z, Wang Z, *et al.* Low cost perovskite quantum dots film based wide color gamut backlight unit for LCD TVs. SID Int Symp Digest Tech Papers, 2018, 49: 1657–1659
19 Zhang Y, Cheng X, Tu D, *et al.* Engineering the bandgap and surface structure of $CsPbCl_3$ nanocrystals to achieve efficient ultraviolet luminescence. Angew Chem Int Ed, 2021, 60: 9693–9698
20 Pradhan N. Journey of making cesium lead halide perovskite nanocrystals: What's next. J Phys Chem Lett, 2019, 10: 5847–5855
21 Pradhan N. Why do perovskite nanocrystals form nanocubes and how can their facets be tuned? A perspective from synthetic prospects. ACS Energy Lett, 2021, 6: 92–99
22 Ji Y, Xu W, Wang Y, *et al.* Supersensitive sensing based on upconversion nanoparticles through cascade photon amplification at single-particle level. Sens Actuat B-Chem, 2022, 367: 132125
23 Jang E, Jun S, Jang H, *et al.* White-light-emitting diodes with quantum dot color converters for display backlights. Adv Mater, 2010, 22: 3076–3080
24 Chang S, Bai Z, Zhong H. *In situ* fabricated perovskite nanocrystals: A revolution in optical materials. Adv Opt Mater, 2018, 6: 1800380
25 Coe-Sullivan S. The quantum dot revolution: Marching towards the mainstream. SID Int Symp Digest Tech Papers, 2016, 47: 239–240
26 Zhang C, Chen J, Wang S, *et al.* Metal halide perovskite nanorods: Shape matters. Adv Mater, 2020, 32: 2002736
27 Yang D, Li P, Zou Y, *et al.* Interfacial synthesis of monodisperse

$CsPbBr_3$ nanorods with tunable aspect ratio and clean surface for efficient light-emitting diode applications. Chem Mater, 2019, 31: 1575–1583
28 Pan G, Bai X, Shen X, *et al.* Bright red YCl_3-promoted $CsPbI_3$ perovskite nanorods towards efficient light-emitting diode. Nano Energy, 2021, 81: 105615
29 Guo J, Hu Q, Lu M, *et al.* Pb^{2+} doped $CsCdBr_3$ perovskite nanorods for pure-blue light-emitting diodes. Chem Eng J, 2022, 427: 131010
30 Dou Y, Cao F, Dudka T, *et al.* Lattice distortion in mixed-anion lead halide perovskite nanorods leads to their high fluorescence anisotropy. ACS Mater Lett, 2020, 2: 814–820
31 Grivas C, Li C, Andreakou P, *et al.* Single-mode tunable laser emission in the single-exciton regime from colloidal nanocrystals. Nat Commun, 2013, 4: 2376
32 Lu WG, Wu XG, Huang S, *et al.* Strong polarized photoluminescence from stretched perovskite-nanocrystal-embedded polymer composite films. Adv Opt Mater, 2017, 5: 1700594
33 Qin J, Wen ZL, Li S, *et al.* Large-scale active luminance film with enhanced polarization made of aligned quantum-rod-containing polymeric nanofibers for highly efficient and wide color gamut LCD displays. Chin J Liq Cryst Disp, 2018, 33: 261–270
34 Sandus O. A review of emission polarization. Appl Opt, 1965, 4: 1634–1642
35 Vezzoli S, Manceau M, Leménager G, *et al.* Exciton fine structure of CdSe/CdS nanocrystals determined by polarization microscopy at room temperature. ACS Nano, 2015, 9: 7992–8003
36 Efros AL, Rosen M, Kuno M, *et al.* Band-edge exciton in quantum dots of semiconductors with a degenerate valence band: Dark and bright exciton states. Phys Rev B, 1996, 54: 4843–4856
37 Bai X, Li H, Peng Y, *et al.* Role of aspect ratio in the photoluminescence of single CdSe/CdS dot-in-rods. J Phys Chem C, 2022, 126: 2699–2707
38 Zhou N, Bekenstein Y, Eisler CN, *et al.* Perovskite nanowire-block copolymer composites with digitally programmable polarization anisotropy. Sci Adv, 2019, 5: eaav8141
39 Wang D, Wu D, Dong D, *et al.* Polarized emission from $CsPbX_3$ perovskite quantum dots. Nanoscale, 2016, 8: 11565–11570
40 Hikmet RAM, Chin PTK, Talapin DV, *et al.* Polarized-light-emitting quantum-rod diodes. Adv Mater, 2005, 17: 1436–1439
41 Xiang H, Wang R, Chen J, *et al.* Research progress of full electroluminescent white light-emitting diodes based on a single emissive layer. Light Sci Appl, 2021, 10: 206
42 Ma Z, Shi Z, Yang D, *et al.* High color-rendering index and stable white light-emitting diodes by assembling two broadband emissive self-trapped excitons. Adv Mater, 2021, 33: 2001367
43 Lu M, Zhang Y, Wang S, *et al.* Metal halide perovskite light-emitting devices: Promising technology for next-generation displays. Adv Funct Mater, 2019, 29: 1902008
44 Lu P, Wu J, Shen X, *et al.* ZnO-Ti_3C_2 MXene electron transport layer for high external quantum efficiency perovskite nanocrystal light-emitting diodes. Adv Sci, 2020, 7: 2001562
45 Li X, Gao X, Zhang X, *et al.* Lead-free halide perovskites for light emission: Recent advances and perspectives. Adv Sci, 2021, 8: 2003334
46 Lu M, Guo J, Sun S, *et al.* Bright $CsPbI_3$ perovskite quantum dot light-emitting diodes with top-emitting structure and a low efficiency roll-off realized by applying zirconium acetylacetonate surface modification. Nano Lett, 2020, 20: 2829–2836
47 Kim YH, Kim S, Kakekhani A, *et al.* Comprehensive defect suppression in perovskite nanocrystals for high-efficiency light-emitting diodes. Nat Photonics, 2021, 15: 148–155
48 Rhee S, Jung D, Kim D, *et al.* Polarized electroluminescence emission in high-performance quantum rod light-emitting diodes *via* the langmuir-blodgett technique. Small, 2021, 17: 2101204
49 Rizzo A, Nobile C, Mazzeo M, *et al.* Polarized light emitting diode by long-range nanorod self-assembling on a water surface. ACS Nano, 2009, 3: 1506–1512
50 Wei Y, Xu Y, Wang Q, *et al.* $CsPbBr_3$ nanowire polarized light-emitting diodes through mechanical rubbing. Chem Commun, 2020, 56: 5413–5416
51 Kim KH, Kim JJ. Origin and control of orientation of phosphorescent and TADF dyes for high-efficiency OLEDs. Adv Mater, 2018, 30: 1705600
52 Nam S, Oh N, Zhai Y, *et al.* High efficiency and optical anisotropy in double-heterojunction nanorod light-emitting diodes. ACS Nano, 2015, 9: 878–885
53 Shi S, Sun LD, Xue YX, *et al.* Scalable direct writing of lanthanide-doped $KMnF_3$ perovskite nanowires into aligned arrays with polarized up-conversion emission. Nano Lett, 2018, 18: 2964–2969
54 Wang J, Fang C, Ma J, *et al.* Aqueous synthesis of low-dimensional lead halide perovskites for room-temperature circularly polarized light emission and detection. ACS Nano, 2019, 13: 9473–9481
55 Granados del Águila A, Liu S, Do TTH, *et al.* Linearly polarized luminescence of atomically thin MoS_2 semiconductor nanocrystals. ACS Nano, 2019, 13: 13006–13014
56 Wang M, Yang Z, Zhang C. Polarized photoluminescence from lead halide perovskites. Adv Opt Mater, 2021, 9: 2002236
57 Hu J, Li L, Yang W, *et al.* Linearly polarized emission from colloidal semiconductor quantum rods. Science, 2001, 292: 2060–2063
58 Chen X, Nazzal A, Goorskey D, *et al.* Polarization spectroscopy of single CdSe quantum rods. Phys Rev B, 2001, 64: 245304
59 Pandya R, Steinmetz V, Puttisong Y, *et al.* Fine structure and spin dynamics of linearly polarized indirect excitons in two-dimensional CdSe/CdTe colloidal heterostructures. ACS Nano, 2019, 13: 10140–10153
60 Planelles J, Rajadell F, Climente JI. Electronic origin of linearly polarized emission in CdSe/CdS dot-in-rod heterostructures. J Phys Chem C, 2016, 120: 27724–27730
61 Lethiec C, Pisanello F, Carbone L, *et al.* Polarimetry-based analysis of dipolar transitions of single colloidal CdSe/CdS dot-in-rods. New J Phys, 2014, 16: 093014
62 Diroll BT, Koschitzky A, Murray CB. Tunable optical anisotropy of seeded CdSe/CdS nanorods. J Phys Chem Lett, 2014, 5: 85–91
63 Smoleński T, Kazimierczuk T, Goryca M, *et al.* Fine structure of an exciton coupled to a single Fe^{2+} ion in a CdSe/ZnSe quantum dot. Phys Rev B, 2017, 96: 155411
64 Talapin DV, Koeppe R, Götzinger S, *et al.* Highly emissive colloidal CdSe/CdS heterostructures of mixed dimensionality. Nano Lett, 2003, 3: 1677–1681
65 Wang J, Gudiksen MS, Duan X, *et al.* Highly polarized photoluminescence and photodetection from single indium phosphide nanowires. Science, 2001, 293: 1455–1457
66 Early KT, McCarthy KD, Odoi MY, *et al.* Linear dipole behavior in single CdSe-oligo(phenylene vinylene) nanostructures. ACS Nano, 2009, 3: 453–461
67 Htoon H, Furis M, Crooker SA, *et al.* Linearly polarized 'fine structure' of the bright exciton state in individual CdSe nanocrystal quantum dots. Phys Rev B, 2008, 77: 035328
68 Jurow MJ, Lampe T, Penzo E, *et al.* Tunable anisotropic photon emission from self-organized $CsPbBr_3$ perovskite nanocrystals. Nano Lett, 2017, 17: 4534–4540
69 Empedocles SA, Neuhauser R, Bawendi MG. Three-dimensional orientation measurements of symmetric single chromophores using polarization microscopy. Nature, 1999, 399: 126–130
70 Chung I, Shimizu KT, Bawendi MG. Room temperature measurements of the 3D orientation of single CdSe quantum dots using polarization microscopy. Proc Natl Acad Sci USA, 2003, 100: 405–408
71 Brokmann X, Ehrensperger MV, Hermier JP, *et al.* Orientational imaging and tracking of single CdSe nanocrystals by defocused microscopy. Chem Phys Lett, 2005, 406: 210–214
72 Yin C, Chen L, Song N, *et al.* Bright-exciton fine-structure splittings in single perovskite nanocrystals. Phys Rev Lett, 2017, 119: 026401
73 Ramade J, Andriambariarijaona LM, Steinmetz V, *et al.* Fine structure of excitons and electron-hole exchange energy in polymorphic $CsPbBr_3$ single nanocrystals. Nanoscale, 2018, 10: 6393–6401
74 Folie BD, Tan JA, Huang J, *et al.* Effect of anisotropic confinement on electronic structure and dynamics of band edge excitons in inorganic perovskite nanowires. J Phys Chem A, 2020, 124: 1867–1876
75 Shinde A, Gahlaut R, Abharana N, *et al.* Implications of the size

variation on the local structure and polarized emission of $CsPbBr_3$ quantum dots. J Mater Sci, 2021, 56: 6977–6986
76 Shi ZF, Li Y, Li S, *et al.* Polarized emission effect realized in $CH_3NH_3PbI_3$ perovskite nanocrystals. J Mater Chem C, 2017, 5: 8699–8706
77 Liu J, Hu F, Zhou Y, *et al.* Polarized emission from single perovskite $FAPbBr_3$ nanocrystals. J Lumin, 2020, 221: 117032
78 Sun JK, Huang S, Liu XZ, *et al.* Polar solvent induced lattice distortion of cubic $CsPbI_3$ nanocubes and hierarchical self-assembly into orthorhombic single-crystalline nanowires. J Am Chem Soc, 2018, 140: 11705–11715
79 Kim H, Kyhm K, Taylor RA, *et al.* Optical shaping of the polarization anisotropy in a laterally coupled quantum dot dimer. Light Sci Appl, 2020, 9: 100
80 Zhang Y, Liu J, Wang Z, *et al.* Synthesis, properties, and optical applications of low-dimensional perovskites. Chem Commun, 2016, 52: 13637–13655
81 Hadar I, Hitin GB, Sitt A, *et al.* Polarization properties of semiconductor nanorod heterostructures: From single particles to the ensemble. J Phys Chem Lett, 2013, 4: 502–507
82 Wu J, Zhang Z, Liu B, *et al.* UV-vis-NIR-driven plasmonic photocatalysts with dual-resonance modes for synergistically enhancing H_2 generation. Sol RRL, 2018, 2: 1800039
83 Siebers B, Biadala L, Yakovlev DR, *et al.* Exciton spin dynamics and photoluminescence polarization of CdSe/CdS dot-in-rod nanocrystals in high magnetic fields. Phys Rev B, 2015, 91: 155304
84 Diroll BT, Gogotsi N, Murray CB. Statistical description of CdSe/CdS dot-in-rod heterostructures using scanning transmission electron microscopy. Chem Mater, 2016, 28: 3345–3351
85 Bera S, Shyamal S, Pradhan N. Chemically spiraling $CsPbBr_3$ perovskite nanorods. J Am Chem Soc, 2021, 143: 14895–14906
86 Carbone L, Nobile C, de Giorgi M, *et al.* Synthesis and micrometer-scale assembly of colloidal CdSe/CdS nanorods prepared by a seeded growth approach. Nano Lett, 2007, 7: 2942–2950
87 Sitt A, Salant A, Menagen G, *et al.* Highly emissive nano rod-in-rod heterostructures with strong linear polarization. Nano Lett, 2011, 11: 2054–2060
88 Hadar I, Philbin JP, Panfil YE, *et al.* Semiconductor seeded nanorods with graded composition exhibiting high quantum-yield, high polarization, and minimal blinking. Nano Lett, 2017, 17: 2524–2531
89 Li Y, Huang H, Xiong Y, *et al.* Using polar alcohols for the direct synthesis of cesium lead halide perovskite nanorods with anisotropic emission. ACS Nano, 2019, 13: 8237–8245
90 Zhao S, Wu J, Chi X, *et al.* Optical properties of inorganic halide perovskite nanorods: Role of anisotropy, temperature, pressure, and nonlinearity. J Phys Chem C, 2022, 126: 2003–2012
91 Zhu X, Dai SW, Lai YL, *et al.* Packing-shape effects of optical properties in amplified spontaneous emission through dynamics of orbit-orbit polarization interaction in hybrid perovskite quantum dots based on self-assembly. J Phys Chem Lett, 2021, 12: 11894–11901
92 Wu J, Cao B, Rino L, *et al.* Strong up-conversion luminescence of rare-earth doped oxide films enhanced by gap modes on ZnO nanowires. Nanoscale, 2018, 10: 726–732
93 Yang G, Zhong H, Bai Z, *et al.* Ultralong homogeneously alloyed $CdSe_xS_{1-x}$ nanowires with highly polarized and color-tunable emissions. Adv Opt Mater, 2014, 2: 885–891
94 Zhang D, Eaton SW, Yu Y, *et al.* Solution-phase synthesis of cesium lead halide perovskite nanowires. J Am Chem Soc, 2015, 137: 9230–9233
95 Zhang D, Yang Y, Bekenstein Y, *et al.* Synthesis of composition tunable and highly luminescent cesium lead halide nanowires through anion-exchange reactions. J Am Chem Soc, 2016, 138: 7236–7239
96 Zhu H, Fu Y, Meng F, *et al.* Lead halide perovskite nanowire lasers with low lasing thresholds and high quality factors. Nat Mater, 2015, 14: 636–642
97 Teunis MB, Jana A, Dutta P, *et al.* Mesoscale growth and assembly of bright luminescent organolead halide perovskite quantum wires. Chem Mater, 2016, 28: 5043–5054
98 Fang G, Lin X, Lin S, *et al.* Permeability of 3D templates plays a considerable role in improving the activity of 3D composite surface-enhanced Raman scattering substrates. J Phys Chem C, 2021, 125: 8323–8332
99 Yu Y, Protasenko V, Jena D, *et al.* Photocurrent polarization anisotropy of randomly oriented nanowire networks. Nano Lett, 2008, 8: 1352–1357
100 Zhang D, Yu Y, Bekenstein Y, *et al.* Ultrathin colloidal cesium lead halide perovskite nanowires. J Am Chem Soc, 2016, 138: 13155–13158
101 Gao Y, Zhao L, Shang Q, *et al.* Ultrathin $CsPbX_3$ nanowire arrays with strong emission anisotropy. Adv Mater, 2018, 30: 1801805
102 Zhou Y, Luo J, Zhao Y, *et al.* Flexible linearly polarized photodetectors based on all-inorganic perovskite $CsPbI_3$ nanowires. Adv Opt Mater, 2018, 6: 1800679
103 Wu J, Zhang Z, Fang Y, *et al.* Plasmon-enhanced photocatalytic cumulative effect on 2D semiconductor heterojunctions towards highly-efficient visible-light-driven solar-to-fuels conversion. Chem Eng J, 2022, 437: 135308
104 Bekenstein Y, Koscher BA, Eaton SW, *et al.* Highly luminescent colloidal nanoplates of perovskite cesium lead halide and their oriented assemblies. J Am Chem Soc, 2015, 137: 16008–16011
105 Hao J, Zhao F, Wang Q, *et al.* Optically active CdSe/CdS nanoplatelets exhibiting both circular dichroism and circularly polarized luminescence. Adv Opt Mater, 2021, 9: 2101142
106 Wu J, Zhang Y, Lu P, *et al.* Engineering 2D multi-hetero-interface in the well-designed nanosheet composite photocatalyst with broad electron-transfer channels for highly-efficient solar-to-fuels conversion. Appl Catal B-Environ, 2021, 286: 119944
107 Davis AH, Zheng W. Discrete composition control of two-dimensional morphologic all-inorganic metal halide perovskite nanocrystals. J Energy Chem, 2021, 59: 257–275
108 Cassette E, Mahler B, Guigner JM, *et al.* Colloidal CdSe/CdS dot-in-plate nanocrystals with 2D-polarized emission. ACS Nano, 2012, 6: 6741–6750
109 Wu J, Lu P, Dai J, *et al.* High performance humidity sensing property of $Ti_3C_2T_x$ MXene-derived $Ti_3C_2T_x/K_2Ti_4O_9$ composites. Sens Actuat B-Chem, 2021, 326: 128969
110 Feng F, NGuyen LT, Nasilowski M, *et al.* Probing the fluorescence dipoles of single cubic CdSe/CdS nanoplatelets with vertical or horizontal orientations. ACS Photonics, 2018, 5: 1994–1999
111 Ma X, Diroll BT, Cho W, *et al.* Anisotropic photoluminescence from isotropic optical transition dipoles in semiconductor nanoplatelets. Nano Lett, 2018, 18: 4647–4652
112 Feng F, Nguyen LT, Nasilowski M, *et al.* Consequence of shape elongation on emission asymmetry for colloidal CdSe/CdS nanoplatelets. Nano Res, 2018, 11: 3593–3602
113 Sheng X, Chen G, Wang C, *et al.* Polarized optoelectronics of $CsPbX_3$ (X = Cl, Br, I) perovskite nanoplates with tunable size and thickness. Adv Funct Mater, 2018, 28: 1800283
114 Zeng Q, Du Y, Jiang J, *et al.* Revealing the aging effect of metal-oleate precursors on the preparation of highly luminescent $CsPbBr_3$ nanoplatelets. J Phys Chem Lett, 2021, 12: 2668–2675
115 Liu L, Huang S, Pan L, *et al.* Colloidal synthesis of $CH_3NH_3PbBr_3$ nanoplatelets with polarized emission through self-organization. Angew Chem Int Ed, 2017, 56: 1780–1783
116 Yang D, Li X, Li Y, *et al.* Facet-induced coordination competition for highly ordered $CsPbBr_3$ nanoplatelets with strong polarized emission. Nano Res, 2022, 15: 502–509
117 Mauser C, Limmer T, da Como E, *et al.* Anisotropic optical emission of single CdSe/CdS tetrapod heterostructures: Evidence for a wavefunction symmetry breaking. Phys Rev B, 2008, 77: 153303
118 Castelli A, Dhanabalan B, Polovitsyn A, *et al.* Core/shell CdSe/CdS bone-shaped nanocrystals with a thick and anisotropic shell as optical emitters. Adv Opt Mater, 2020, 8: 1901463
119 Ge Y, Zhang M, Wang L, *et al.* Polarization-sensitive ultraviolet detection from oriented-CdSe@CdS-dot-in-rods-integrated silicon photodetector. Adv Opt Mater, 2019, 7: 1900330
120 Gupta SK, Prodanov MF, Zhang W, *et al.* Inkjet-printed aligned quantum rod enhancement films for their application in liquid crystal displays. Nanoscale, 2019, 11: 20837–20846

121 Zhou Z, Wang K, Zhang Z, *et al.* Highly polarized fluorescent film based on aligned quantum rods by contact ink-jet printing method. IEEE Photonics J, 2019, 11: 1–11
122 He J, Towers A, Wang Y, *et al. In situ* synthesis and macroscale alignment of $CsPbBr_3$ perovskite nanorods in a polymer matrix. Nanoscale, 2018, 10: 15436–15441
123 Raja SN, Bekenstein Y, Koc MA, *et al.* Encapsulation of perovskite nanocrystals into macroscale polymer matrices: Enhanced stability and polarization. ACS Appl Mater Interfaces, 2016, 8: 35523–35533
124 Wang J, Zhang Y, Chen J, *et al.* Strong polarized photoluminescence $CsPbBr_3$ nanowire composite films for UV spectral conversion polarization photodetector enhancement. ACS Appl Mater Interfaces, 2021, 13: 36147–36156
125 Ercan E, Liu CL, Chen WC. Nano-micro dimensional structures of fiber-shaped luminous halide perovskite composites for photonic and optoelectronic applications. Macromol Rapid Commun, 2020, 41: 2000157
126 Xue J, Wu T, Dai Y, *et al.* Electrospinning and electrospun nanofibers: Methods, materials, and applications. Chem Rev, 2019, 119: 5298–5415
127 Tsai PC, Chen JY, Ercan E, *et al.* Uniform luminous perovskite nanofibers with color-tunability and improved stability prepared by one-step core/shell electrospinning. Small, 2018, 14: 1704379
128 Li QF, Wang JT, Tian B, *et al.* Hybridization of $CsPbBr_3$ perovskite nanocrystals with polymer nanofiber to improve their luminescence stability. Eur J Inorg Chem, 2018, 2018: 4215–4220
129 Lin CC, Jiang DH, Kuo CC, *et al.* Water-resistant efficient stretchable perovskite-embedded fiber membranes for light-emitting diodes. ACS Appl Mater Interfaces, 2018, 10: 2210–2215
130 Wang Y, Zhu Y, Huang J, *et al.* $CsPbBr_3$ perovskite quantum dots-based monolithic electrospun fiber membrane as an ultrastable and ultrasensitive fluorescent sensor in aqueous medium. J Phys Chem Lett, 2016, 7: 4253–4258
131 Wu MC, Kao CK, Lin TF, *et al.* Surface plasmon resonance amplified efficient polarization-selective volatile organic compounds CdSe-CdS/Ag/PMMA sensing material. Sens Actuat B-Chem, 2020, 309: 127760
132 Jiang T, Wang J, Xie L, *et al. In situ* fabrication of lead-free $Cs_3Cu_2I_5$ nanostructures embedded in poly(vinylidene fluoride) electrospun fibers for polarized emission. ACS Appl Nano Mater, 2022, 5: 508–516
133 Meng L, Yang C, Meng J, *et al. In-situ* fabricated anisotropic halide perovskite nanocrystals in polyvinylalcohol nanofibers: Shape tuning and polarized emission. Nano Res, 2019, 12: 1411–1416
134 Wang Y, Jia S, Luo W, *et al.* Inch-sized aligned polymer nanofiber films with embedded $CH_3NH_3PbBr_3$ nanocrystals: Electrospinning fabrication using a folded aluminum foil as the collector. Nanotechnology, 2019, 31: 075708
135 Güner T, Topçu G, Savacı U, *et al.* Polarized emission from $CsPbBr_3$ nanowire embedded-electrospun PU fibers. Nanotechnology, 2018, 29: 135202
136 Hasegawa M, Hirayama Y, Dertinger S. Polarized fluorescent emission from aligned electrospun nanofiber sheets containing semiconductor nanorods. Appl Phys Lett, 2015, 106: 051103
137 Aubert T, Palangetic L, Mohammadimasoudi M, *et al.* Large-scale and electroswitchable polarized emission from semiconductor nanorods aligned in polymeric nanofibers. ACS Photonics, 2015, 2: 583–588
138 Schneider J, Zhang W, Srivastava AK, *et al.* Photoinduced micropattern alignment of semiconductor nanorods with polarized emission in a liquid crystal polymer matrix. Nano Lett, 2017, 17: 3133–3138
139 Zhang W, Schneider J, Chigrinov VG, *et al.* Optically addressable photoaligned semiconductor nanorods in thin liquid crystal films for display applications. Adv Opt Mater, 2018, 6: 1800250
140 Pelliser L, Manceau M, Lethiec C, *et al.* Alignment of rod-shaped single-photon emitters driven by line defects in liquid crystals. Adv Funct Mater, 2015, 25: 1719–1726
141 Amit Y, Faust A, Lieberman I, *et al.* Semiconductor nanorod layers aligned through mechanical rubbing. Phys Status Solidi A, 2012, 209: 235–242
142 Lee DM, Lee YJ, Kim JH, *et al.* Birefringence-dependent linearly-polarized emission in a liquid crystalline organic light emitting polymer. Opt Express, 2017, 25: 3737–3742
143 Kim J, Peretti J, Lahlil K, *et al.* Optically anisotropic thin films by shear-oriented assembly of colloidal nanorods. Adv Mater, 2013, 25: 3295–3300
144 Deng H, Dong D, Qiao K, *et al.* Growth, patterning and alignment of organolead iodide perovskite nanowires for optoelectronic devices. Nanoscale, 2015, 7: 4163–4170
145 Liu H, Siron M, Gao M, *et al.* Lead halide perovskite nanowires stabilized by block copolymers for Langmuir-Blodgett assembly. Nano Res, 2020, 13: 1453–1458
146 Hu Z, Fischbein MD, Querner C, *et al.* Electric-field-driven accumulation and alignment of CdSe and CdTe nanorods in nanoscale devices. Nano Lett, 2006, 6: 2585–2591
147 Kaur S, Murali G, Manda R, *et al.* Functional film with electric-field-aided aligned assembly of quantum rods for potential application in liquid crystal display. Adv Opt Mater, 2018, 6: 1800235
148 Persano A, De Giorgi M, Fiore A, *et al.* Photoconduction properties in aligned assemblies of colloidal CdSe/CdS nanorods. ACS Nano, 2010, 4: 1646–1652
149 Gryn I, Lacaze E, Carbone L, *et al.* Electric-field-controlled alignment of rod-shaped fluorescent nanocrystals in smectic liquid crystal defect arrays. Adv Funct Mater, 2016, 26: 7122–7131
150 Mohammadimasoudi M, Beeckman J, Hens Z, *et al.* Hybrid fluorescent layer emitting polarized light. APL Mater, 2017, 5: 076104
151 Wang T, Zhuang J, Lynch J, *et al.* Self-assembled colloidal superparticles from nanorods. Science, 2012, 338: 358–363
152 Deng W, Huang L, Xu X, *et al.* Ultrahigh-responsivity photodetectors from perovskite nanowire arrays for sequentially tunable spectral measurement. Nano Lett, 2017, 17: 2482–2489
153 Lutich A, Carbone L, Volchek S, *et al.* Macroscale alignment of CdSe/CdS nanorods by porous anodic alumina templates. Phys Stat Sol (RRL), 2009, 3: 151–153
154 Yuan Y, Giri G, Ayzner AL, *et al.* Ultra-high mobility transparent organic thin film transistors grown by an off-centre spin-coating method. Nat Commun, 2014, 5: 3005
155 Wang J, Wei Y, Xu Y, *et al.* Photoluminescence and electroluminescence properties of aligned $CsPbBr_3$ nanowire films prepared by off-center spin-coating. Synth Met, 2020, 267: 116481
156 Kim NK, Jang SY, Pace G, *et al.* High-performance organic field-effect transistors with directionally aligned conjugated polymer film deposited from pre-aggregated solution. Chem Mater, 2015, 27: 8345–8353
157 Kang L, Chen H, Yang ZJ, *et al.* Seesaw-like polarized transmission behavior of silver nanowire arrays aligned by off-center spin-coating. J Appl Phys, 2018, 123: 205110
158 Lee G, Kim H, Lee SB, *et al.* Tailored uniaxial alignment of nanowires based on off-center spin-coating for flexible and transparent field-effect transistors. Nanomaterials, 2022, 12: 1116
159 Anzai T, Porzio W, Vohra V. Polarized emission from conjugated polymer chains aligned by epitaxial growth during off-center spin-coating. J Chem, 2017, 2017: 1–9
160 Zhang GF, Yang CG, Ge Y, *et al.* Influence of surface charges on the emission polarization properties of single CdSe/CdS dot-in-rods. Front Phys, 2019, 14: 63601
161 Chen S, Cao W, Liu T, *et al.* On the degradation mechanisms of quantum-dot light-emitting diodes. Nat Commun, 2019, 10: 765
162 Ali S, Chang S, Imran M, *et al.* Impedance spectroscopy: A versatile technique to understand solution-processed optoelectronic devices. Phys Status Solidi RRL, 2019, 13: 1800580
163 Xu M, Peng Q, Zou W, *et al.* A transient-electroluminescence study on perovskite light-emitting diodes. Appl Phys Lett, 2019, 115: 041102
164 Han TH, Kim YH, Kim MH, *et al.* Synergetic influences of mixed-host emitting layer structures and hole injection layers on efficiency and lifetime of simplified phosphorescent organic light-emitting diodes. ACS Appl Mater Interfaces, 2016, 8: 6152–6163

Acknowledgements This work was supported by the European Union's Horizon 2020 Research and Innovation Programme under the Marie Skło-

dowska-Curie grant agreement (801165), with co-funding through Science Foundation Ireland, Career Development Award (17/CDA/4733). The work was also supported by the National Natural Science Foundation of China (12204088, 11974069 and U21A2074), Liaoning Revitalization Talents Program (XLYC1902113), and the Science and Technology Project of Liaoning Province (2020JH2/10100012).

Funding note Open Access funding provided by the IReL Consortium.

Author contributions Wu J, Fang G, Zhang Y and Biswas N collected and summarized the literature. Wu J wrote the original manuscript. Ji Y and Xu W developed the concept and offered creative proposal for improving the depth of the review. Dong B and Liu N supervised the project. Liu N revised the manuscript. All authors contributed to the general discussion.

Conflict of interest The authors declare that they have no conflict of interest.

Jinlei Wu received his PhD degree in 2021, from the College of Electrical Science and Engineering, Jilin University, China. He has been a lecturer at Dalian Minzu University since 2021. He got Marie Skłodowska-Curie COFUND Postdoctoral Fellowship and has been working as a postdoctoral researcher at the University of Limerick since 2022. His research interest mainly focuses on luminescent nanomaterials, semiconductor optoelectronic devices and plasmonic nanostructures.

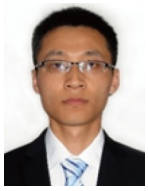

Wen Xu was born and raised in Sichuan, China, and earned his BS degree from Jilin University. Then, he received his PhD degree from Jilin University in 2014 under the supervision of Professor Hongwei Song. From 2015 to 2018, he worked as a postdoctoral researcher at Nanyang Technological University, Singapore, and Japan Science Promotion Society (JSPS) postdoctoral researcher at Tokyo Institute of Technology, Japan, respectively. Currently, he is a professor at Dalian Minzu University. His research interests focus on nano-luminescent materials and their applications in photoelectric devices.

Bin Dong is a professor at the School of Physics and Materials Engineering, Dalian Minzu University. He received his PhD degree from Dalian University of Technology in 2007. From 2008 to 2011, he worked as a postdoctoral researcher at the Institute of Physics, Chinese Academy of Sciences (CAS). He is mainly engaged in the fundamental and application research of rare earth functional materials.

Ning Liu is a senior lecturer in nanophysics at the Department of Physics, University of Limerick. She received her BSc degree in physics from Peking University in 1999 and PhD degree in physics from the University of California at Irvine in 2005. Ning Liu has expertise in scanning probe microscopy, ultrafast pump-probe microscopy and other linear and nonlinear optical techniques. Her current research interests are in electrically pumped nanocrystal-based light emitting diodes, spin-orbit coupling of light, nanophotonics and nanoplasmonics.

基于半导体纳米材料的偏振光发射: 从材料到发光二极管

吴金磊[1,2], 方国强[2], 张永亮[1], Nandita Biswas[1], 季亚楠[2], 徐文[2], 董斌[2*], 刘宁[1*]

摘要 由于偏光片、彩色滤光片和液晶层等结构的损耗, 基于背光源技术的液晶显示器的整体效率不足5%. 自发射发光二极管(LED)不但具有巨大的市场潜力, 而且能够满足未来显示的需求, 迎来了巨大的发展机遇. 更重要的是, 由于避免了偏光片造成的光损失, 偏振LED可以提高背景光利用效率. 因此, 亟需寻找有效的方法组装高质量的各向异性纳米材料薄膜, 从而制备出具有高偏振度和高外量子效率的偏振LED. 本文介绍了一些半导体纳米材料的光电特性及其在偏振LED中的潜在应用. 综述了在偏振光发射领域从材料到薄膜, 再到LED的研究进展; 总结和比较了构建偏振光发射薄膜和LED的不同组装策略; 最后, 讨论了当前面临的挑战, 并对偏振LED的潜在商业应用价值进行了展望. 我们希望这篇综述能够对偏振LED当前研究进展进行有价值的总结, 并对其未来发展激发一些新的、切实可行的想法.